

Accuracy and precision of objective refraction from wavefront aberrations

Larry N. Thibos

School of Optometry, Indiana University, Bloomington, IN, USA



Xin Hong

School of Optometry, Indiana University, Bloomington, IN, USA

Arthur Bradley

School of Optometry, Indiana University, Bloomington, IN, USA



Raymond A. Applegate

College of Optometry, University of Houston, Houston, TX, USA



We determined the accuracy and precision of 33 objective methods for predicting the results of conventional, spherocylindrical refraction from wavefront aberrations in a large population of 200 eyes. Accuracy for predicting defocus (as specified by the population mean error of prediction) varied from -0.50 D to +0.25 D across methods. Precision of these estimates (as specified by 95% limits of agreement) ranged from 0.5 to 1.0 D. All methods except one accurately predicted astigmatism to within $\pm 1/8$ D. Precision of astigmatism predictions was typically better than precision for predicting defocus and many methods were better than 0.5D. Paraxial curvature matching of the wavefront aberration map was the most accurate method for determining the spherical equivalent error whereas least-squares fitting of the wavefront was one of the least accurate methods. We argue that this result was obtained because curvature matching is a biased method that successfully predicts the biased endpoint stipulated by conventional refractions. Five methods emerged as reasonably accurate and among the most precise. Three of these were based on pupil plane metrics and two were based on image plane metrics. We argue that the accuracy of all methods might be improved by correcting for the systematic bias reported in this study. However, caution is advised because some tasks, including conventional refraction of defocus, require a biased metric whereas other tasks, such as refraction of astigmatism, are unbiased. We conclude that objective methods of refraction based on wavefront aberration maps can accurately predict the results of subjective refraction and may be more precise. If objective refractions are more precise than subjective refractions, then wavefront methods may become the new gold standard for specifying conventional and/or optimal corrections of refractive errors.

Keywords: visual optics, optical aberrations, refraction, metrics of optical quality

Introduction

The purpose of a conventional, ophthalmic refraction of the eye is to determine that combination of spherical and cylindrical lenses which optimizes visual acuity for distant objects. The underlying assumption of refraction is that visual acuity is maximized when the quality of the retinal image is maximized. Furthermore, it is commonly assumed that retinal image quality is maximized when the image is optimally focused. For these reasons, the endpoint of a subjective refraction is taken as an operational definition of the term "best correction" as applied to eyes.

This paper is concerned with the problem of objectively determining the best correction of an eye from measurements of wavefront aberrations. Aberrometers measure all of the eye's monochromatic aberrations and display the result in the form of an aberration map that describes the variation in optical path length from source to retinal image through each point in the pupil. Zernike expansion of an aberration map includes the second order aberrations of defocus and astigmatism. Thus, one obvious strategy for

objective refraction is to prescribe correcting lenses based on Zernike coefficients of the second-order.

Unfortunately, the problem is not solved so easily. Several studies have shown that eliminating the second-order Zernike aberrations does not necessarily optimize the subjective impression of best-focus nor the objective measurement of visual performance (Applegate, Ballantine, Gross, Sarver, & Sarver, 2003; Applegate, Marsack, Ramos, & Sarver, 2003; Guirao & Williams, 2003; Thibos, Hong, Bradley, & Cheng, 2002). Eliminating second-order Zernike aberrations is equivalent to minimizing the root mean squared (RMS) wavefront error, but this minimization does not necessarily optimize the quality of the retinal image (King, 1968; Mahajan, 1991). Thus a search has begun for alternative metrics of optical quality that are optimized by subjective refraction when higher-order aberrations are present.

A variety of problems must be solved when converting an aberration map into a prescription for corrective lenses or refractive surgery. One of the most important is a correction for the eye's chromatic aberration. Objective aber-

rometers typically use infrared light, for which the eye has relatively low refractive power compared to visible light. Optical models of longitudinal chromatic aberration (Thibos, Ye, Zhang, & Bradley, 1992) can be extrapolated to estimate the difference in optical power of the eye between the measurement wavelength and some visible wavelength, but it is unclear what wavelength should be chosen as a reference for any given eye. Furthermore, since only one wavelength can be in-focus at a time, some method is needed to factor in the relative contribution of all wavelengths, each with a different amount of defocus and a different luminance, in order to objectively refract an eye for polychromatic objects.

Another sticky problem is the lack of a universally accepted metric of image quality that could be used to establish objectively the state of optimum-focus for an aberrated eye. One purpose of this paper is to describe a variety of such metrics based on general principles described elsewhere (Cheng, Thibos, & Bradley, 2003; Williams, Applegate, & Thibos, 2004). Assuming that consensus agreement could be achieved for a metric of choice, one still needs to deal with the fact that identifying the best correction is a multi-dimensional problem in optimization. Guirao & Williams (Guirao & Williams, 2003) have described an iterative method for finding the optimum sphere, cylinder and axis parameters that optimize a metric of image quality. Other possibilities include an objective version of the clinical technique of refraction by successive elimination. A first

approximation would eliminate the bulk of defocus error by correcting the eye with a spherical lens of power M , the so-called spherical equivalent. Next, the eye's astigmatism is corrected with a cylindrical lens, followed by a fine-tuning of the spherical lens power if necessary. This is the basis of most of the methods described below.

A different kind of problem is to incorporate into the method the refractionist's rule "maximum plus to best visual acuity" (Borisch, 1970). According to this clinical maxim, the spherical refractive error of myopic eyes should be deliberately under-corrected. The amount of under-correction is not enough to diminish visual acuity, but it is sufficient to minimize unnecessary accommodation and to maximize the usable depth of focus (DOF) at distance and near. These twin goals are achieved by prescribing a spherical lens power that is slightly less negative (in the case of myopia) or slightly more positive (in the case of hyperopia) than the lens required to make the retina conjugate to infinity. Instead, the prescribed lens conjugates the retina with a plane at the hyperfocal distance, which is the nearest distance the retina can focus on without significantly reducing visual performance for a target located at infinity (Campbell, 1957). Consequently, the eye is left in a slightly myopic state (Figure 1B), compared to an optimum correction that would place the retina conjugate to infinity (Figure 1A). Note that the diagram in Figure 1 has been simplified by assuming that any astigmatism has already been fully corrected using the appropriate cylindrical lens.

Yet another issue is the extent to which neural factors need to be taken into account when converting an aberration map into a prescription. One such neural factor is the angular sensitivity of cone photoreceptors (Enoch & Lakshminarayanan, 1991) which is commonly modeled optically by an apodization filter in the pupil plane (Bradley & Thibos, 1995; Metcalf, 1965). Post-receptorial neural processing of the retinal image affects the processing of blurred retinal images in a manner that can be modeled as a mathematical convolution of the optical point-spread function with a neural point-spread function (Thibos & Bradley, 1995). This too may be construed as a form of apodization since the effect of the convolution will be to attenuate the remote tails of a blurred point-spread function (PSF).

Recently Guirao and Williams (Guirao & Williams, 2003) described a variety of methods for quantifying the optical quality of an eye based on (1) analysis of wavefront aberrations using pupil-plane metrics and (2) analysis of retinal image quality using image-plane metrics. They reported that all five image plane metrics they considered were more accurate than two pupil-plane metrics in predicting the optimum subjective refraction for a polychromatic target for a small population of 6 eyes. Further testing was done on a large population of 146 eyes for which aberration data for a fixed, 5.7 mm pupil were available in the literature. Unfortunately, a variety of uncontrolled conditions precluded strong conclusions from this large population (e.g. possible fluctuations of accommodation, un-

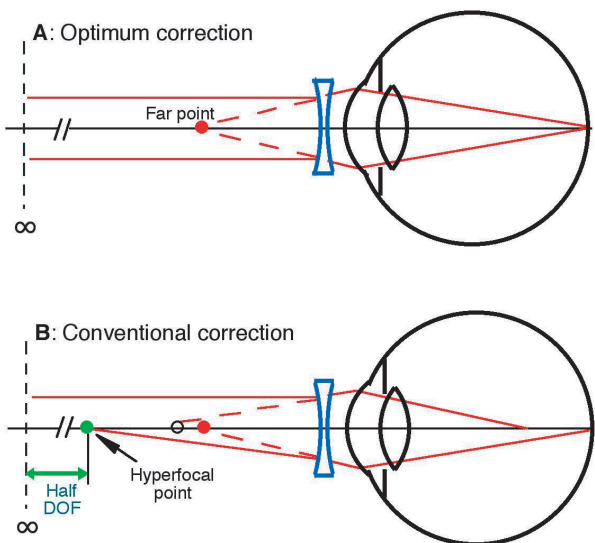


Figure 1. Two criteria for refraction. (A) An optimum refraction conjugates the retina with infinity. In this case the ideal correcting lens images infinity at the eye's far point (•). (B) A conventional refraction conjugates the fovea with the eye's hyperfocal point (•), which lies closer to the eye by an amount equal to half the depth-of-field (DOF). In this case the correcting lens images infinity at a point (o) slightly beyond the eye's far point and therefore the eye remains slightly myopic.

known pupil size during subjective refraction, binocular refractions that likely yielded sub-optimal acuity endpoints) but nevertheless the authors found a close correlation between subjective and objective refractions computed from image-plane metrics. Although visual performance during refraction presumably depended on some combination of optical and neural factors, they found that optimizing the optical image without considering neural factors led to accurate prediction of the outcome of subjective refraction. However, no assessment of the precision of these predictions was reported.

The purpose of our study was to evaluate two general approaches to converting an aberration map into a conventional spherocylindrical prescription. The first approach is a surface-fitting procedure designed to find the nearest spherocylindrical approximation to the actual wavefront aberration map. The second approach involves a virtual through-focus experiment in which the computer adds or subtracts various amounts of spherical or cylindrical wavefronts to the aberration map until the optical quality of the eye is maximized. Preliminary accounts of this work have been presented (Thibos, Bradley, & Applegate, 2002; Thibos, Hong, & Bradley, 2001).

Methods

Refraction based on the principle of equivalent quadratic

We define the *equivalent quadratic* of a wavefront aberration map as that quadratic (i.e. a spherocylindrical) surface which best represents the map. This idea of approximating an arbitrary surface with an equivalent quadratic is a simple extension of the common ophthalmic technique of approximating a spherocylindrical surface with an equivalent sphere. Two methods for determining the equivalent quadratic from an aberration map are presented next.

Least-squares fitting

One common way to fit an arbitrarily aberrated wavefront with a quadratic surface is to minimize the sum of squared deviations between the two surfaces. This least-squares fitting method is the basis for Zernike expansion of wavefronts. Because the Zernike expansion employs an orthogonal set of basis functions, the least-squares solution is given by the second-order Zernike coefficients, regardless of the values of the other coefficients. These second-order Zernike coefficients can be converted to a spherocylindrical prescription in power vector notation using Equation 1,

$$\begin{aligned} M &= \frac{-c_2^0 4\sqrt{3}}{r^2} \\ J_0 &= \frac{-c_2^2 2\sqrt{6}}{r^2} \\ J_{45} &= \frac{-c_2^{-2} 2\sqrt{6}}{r^2} \end{aligned} \quad (1)$$

where c_n^m is the n^{th} order Zernike coefficient of meridional frequency m , and r is pupil radius. The power vector notation is a cross-cylinder convention that is easily transposed into conventional minus-cylinder or plus-cylinder formats used by clinicians (see equations 22, 23 of Thibos, Wheeler, & Horner, 1997).

Paraxial curvature matching

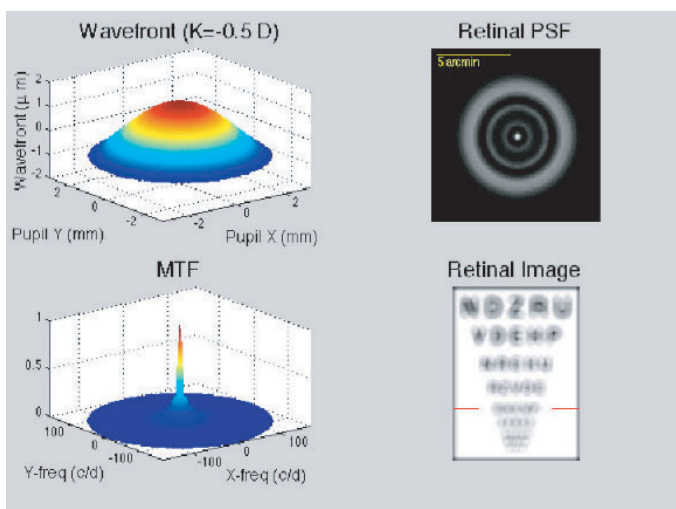
Curvature is the property of wavefronts that determines how they focus. Thus, another reasonable way to fit an arbitrary wavefront with a quadratic surface is to match the curvature of the two surfaces at some reference point. A variety of reference points could be selected, but the natural choice is the pupil center. Two surfaces that are tangent at a point and have exactly the same curvature in every meridian are said to osculate. Thus, the surface we seek is the *osculating quadric*. Fortunately, a closed-form solution exists for the problem of deriving the power vector parameters of the osculating quadratic from the Zernike coefficients of the wavefront (Thibos et al., 2002). This solution is obtained by computing the curvature at the origin of the Zernike expansion of the Seidel formulae for defocus and astigmatism. This process effectively collects all r^2 terms from the various Zernike modes. We used the OSA definitions of the Zernike polynomials, each of which has unit variance over the unit circle (Thibos, Applegate, Schwiegerling, & Webb, 2000). The results given in Equation 2 are truncated at the sixth Zernike order but could be extended to higher orders if warranted.

$$\begin{aligned} M &= \frac{-c_2^0 4\sqrt{3} + c_4^0 12\sqrt{5} - c_6^0 24\sqrt{7} + \dots}{r^2} \\ J_0 &= \frac{-c_2^2 2\sqrt{6} + c_4^2 6\sqrt{10} - c_6^2 12\sqrt{14} + \dots}{r^2} \\ J_{45} &= \frac{-c_2^{-2} 2\sqrt{6} + c_4^{-2} 6\sqrt{10} - c_6^{-2} 12\sqrt{14} + \dots}{r^2} \end{aligned} \quad (2)$$

Refraction based on maximizing optical or visual quality

An empirical way to determine the focus error of an eye (with accommodation paralyzed) is to move an object axially along the line-of-sight until the retinal image of that object appears subjectively to be well focused. This procedure is easily simulated mathematically by adding a spherical wavefront to the eye's aberration map and then comput-

ing the retinal image using standard methods of Fourier optics as illustrated in [Movie 1](#). The curvature of the added wavefront can be systematically varied to simulate a through-focus experiment that varies the optical quality of the eye+lens system over a range from good to bad. Given a suitable metric of optical quality, this computational procedure yields the optimum power M of that spherical correcting lens needed to maximize optical quality of the corrected eye. With this virtual spherical lens in place, the process can be repeated for through-astigmatism calculations to determine the optimum values of J_0 and J_{45} needed to maximize image quality. If necessary, a second iteration could be used to fine-tune results by repeating the above process with these virtual lenses in place. However, the analysis reported below did not include a second iteration.



Movie 1. Dynamic simulation of the through-focus method of objective refraction. To determine the optimum value M of a spherical defocusing lens, a pre-determined sequence of M -values are used to modulate the wavefront map in the same way that a real lens alters the eye's wavefront aberration function. From the new aberration map we compute the retinal point-spread function (PSF), optical transfer function (OTF), and retinal image of an eye chart. Scalar metrics of optical quality are used to optimize focus (M). The process is then repeated to optimize astigmatism parameters J_0 , J_{45} . This example is for an eye with $0.1 \mu\text{m}$ of spherical aberration.

The computational method described above captures the essence of clinical refraction by mathematically simulating the effects of spherocylindrical lenses of various powers. Our method is somewhat simpler to implement than that described by Guirao & Williams (Guirao & Williams, [2003](#)) who used an iterative searching method to determine that combination of spherical and cylindrical lenses which maximizes the eye's optical quality. Regardless of which searching algorithm is used, a suitable metric of optical quality is required as a merit function. Guirao and Williams used 5 such metrics of image quality. In [Appendix A](#) we expand their list to 31 metrics by systematically pursuing three general approaches to quantifying optical quality: (1)

wavefront quality, (2) retinal image quality for point objects, and (3) retinal image quality for grating objects. Implementation of image sharpness metrics for extended objects, such as a letter chart, (Fienup & Miller, [2003](#); Hultgren, [1990](#)) have been left for future work. Several of the implemented metrics include a neural component that takes into account the spatial filtering of the retinal image imposed by the observer's visual system. Strictly speaking, such metrics should be referred to as metrics of neuro-optical quality or visual quality, but for simplicity we use the term "optical quality metric" generically. For each of these 31 metrics we used the virtual refraction procedure described above to determine (to the nearest $1/8$ D) the values of M , J_0 and J_{45} required to maximize the metric. These objective refractions were then compared with conventional subjective refractions. A listing of acronyms for the various refraction methods is given in [Table 1](#).

Evaluation of methods for objective refraction

To judge the success of an objective method of refraction requires a gold standard for comparison. The most clinically relevant choice is a subjective refraction performed for Sloan letter charts illuminated by white light. Accordingly, we evaluated our objective refractions against the published results of the Indiana Aberration Study (Thibos et al., [2002](#)). That study yielded a database of aberration maps for 200 eyes that were subjectively well-corrected by clinical standards. The methodology employed avoided the problems mentioned above that limited the conclusions drawn by Guirao & Williams. A brief summary of the experimental procedure used in the Indiana Aberration Study is given next.

Subjective refractions were performed to the nearest 0.25D on 200 normal, healthy eyes from 100 subjects using the standard optometric protocol of maximum plus to best visual acuity. Accommodation was paralyzed with 1 drop of 0.5% cyclopentolate during the refraction. Optical calculations were performed for the fully dilated pupil, which varied between 6-9 mm for different eyes. The refractive correction was taken to be that spherocylindrical lens combination which optimally corrected astigmatism and conjugated the retina with the eye's hyperfocal point ([Figure 1b](#)). This prescribed refraction was then implemented with trial lenses and worn by the subject during subsequent aberrometry ($\lambda = 633$ nm). This experimental design emphasized the effects of higher-order aberrations by minimizing the presence of uncorrected second-order aberrations. The eye's longitudinal chromatic aberration was taken into account by the different working distances used for aberrometry and subjective refraction as illustrated in [Figure 2](#). Assuming the eye was well focused for 570 nm when viewing the polychromatic eye chart at 4 m, the eye would also have been focused at infinity for the 633nm laser light used for aberrometry (Thibos et al., [1992](#)).

N	Acronym	Brief Description
1	RMSw	Standard deviation of wavefront
2	PV	Peak-valley
3	RMSs	RMSs: std(slope)
4	PFWc	Pupil fraction for wavefront (critical pupil)
5	PFWt	Pupil fraction for wavefront (tessellation)
6	PFSt	Pupil fraction for slope (tessellation)
7	PFSc	Pupil fraction for slope (critical pupil)
8	Bave	Average Blur Strength
9	PFCT	Pupil fraction for curvature (tessellation)
10	PFCC	Pupil fraction for curvature (critical pupil)
11	D50	50% width (min)
12	EW	Equivalent width (min)
13	SM	Sqrt(2nd moment) (min)
14	HWHH	Half width at half height (arcmin)
15	CW	Correlation width (min)
16	SRX	Strehl ratio in space domain
17	LIB	Light in the bucket (norm)
18	STD	Standard deviation of intensity (norm)
19	ENT	Entropy (bits)
20	NS	Neural sharpness (norm)
21	VSX	Visual Strehl in space domain
22	SFCMTF	Cutoff spat. freq. for rMTF (c/d)
23	AreaMTF	Area of visibility for rMTF (norm)
24	SFCOTF	Cutoff spat. freq. for rOTF (c/d)
25	AreaOTF	Area of visibility for rOTF (norm)
26	SROTF	Strehl ratio for OTF
27	VOTF	OTF vol/ MTF vol
28	VSOTF	Visual Strehl ratio for OTF
29	VNOTF	CS*OTF vol/ CS*MTF vol
30	SRMTF	Strehl ratio for MTF
31	VSMTF	Visual Strehl ratio for MTF
32	LSq	Least squares fit
33	Curve	Curvature fit

Table 1. Listing of acronyms for refraction methods. Ordering is that used in correlation matrices (Figures 8, A8).

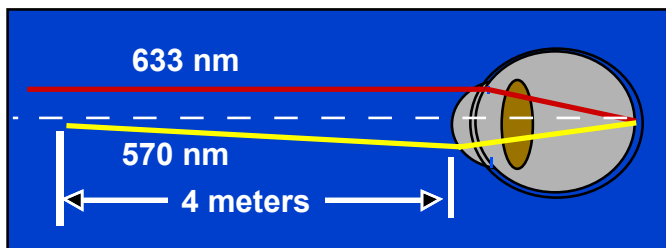


Figure 2. Schematic diagram of optical condition of the Indiana Aberration Study. Yellow light with 570 nm wavelength is assumed to be in focus during subjective refraction with a white-light target at 4 m. At the same time, 633 nm light from a target at infinity would be well focused because of the eye's longitudinal chromatic aberration.

Since all eyes were corrected with spectacle lenses during aberrometry, the predicted refraction was $M = J_0 = J_{45} = 0$. The level of success achieved by the 33 methods of objective refraction described above was judged on the basis of precision and accuracy at matching these predictions

(Figure 3). Accuracy for the spherical component of refraction was computed as the population mean of M as determined from objective refractions. Accuracy for the astigmatic component of refraction was computed as the population mean of (Bullimore, Fusaro, & Adams, 1998) vectors. Precision is a measure of the variability in results and is defined for M as twice the standard deviation of the population values, which corresponds to the 95% limits of agreement (LOA) (Bland & Altman, 1986). The confidence region for astigmatism is an ellipse computed for the bivariate distribution of J_0 and J_{45} . This suggests a definition of precision as the geometric mean of the major and minor axes of the 95% confidence ellipse.

In our view, accuracy and precision are equally important for refraction. A method that is precise but not accurate will yield the same wrong answer every time. Conversely, a method that is accurate but not precise gives different answers every time and is correct only on average. Thus we seek a method that is both accurate and precise. However, one might argue that lack of accuracy implies a systematic bias that could be removed by a suitable correction factor applied to any individual eye. One way to obtain such a correction factor is to examine the population statistics of a large number of eyes, as we have done in this study. Any systematic bias obtained for this group could then be used as a correction factor for future refractions, assuming of course that the individual in question is well represented by the population used to determine the correction factor. Although this may be an expedient solution

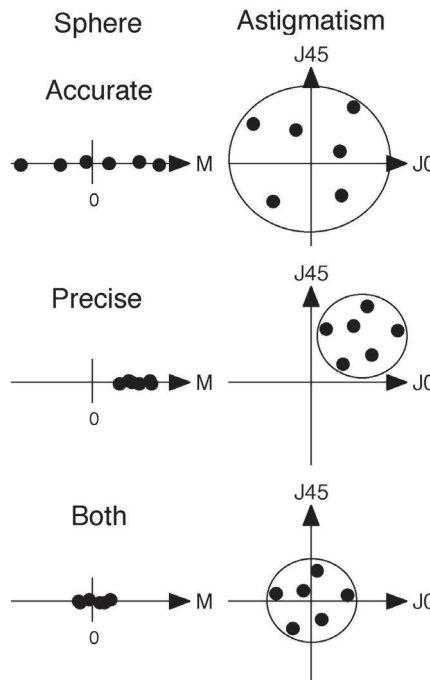


Figure 3. Graphical depiction of the concepts of precision and accuracy as applied to the 1-dimensional problem of estimating spherical power (left column of diagrams) and the 2-dimensional problem of estimating astigmatism (right column of diagrams).

to the problem of objective refraction, it lacks the power of a theoretically sound account of the reasons for systematic biases in the various metrics of optical quality.

Results

Refraction based on equivalent quadratic

The two methods for determining the equivalent quadratic surface for a wavefront aberration map gave consistently different results. A frequency histogram of results for the least-squares method (Figure 4A) indicated an average spherical refractive error of $M = -0.39$ D. In other words, this objective method predicted the eyes were, on average, significantly myopic compared to subjective refraction. To the contrary, the method based on paraxial curvature matching (Figure 4B) predicted an average refractive error close to zero for our population. Both methods accurately predicted the expected astigmatic refraction as shown by the scatter plots and 95% confidence ellipses in Figure 5.

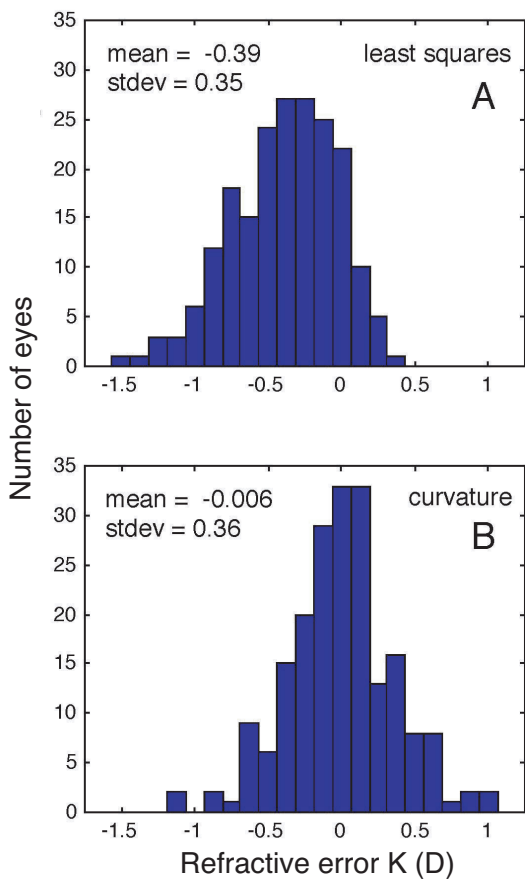


Figure 4. Frequency distribution of results for the least-squares method for fitting the wavefront aberration map with a quadratic surface. Dilated pupil size ranged from 6 to 9 mm across the population.

Refraction based on maximizing optical or visual quality

Computer simulation of through-focus experiments to determine that lens (either spherical or astigmatic) which optimizes image quality are computationally intensive, producing many intermediate results of interest but too voluminous to present here. One example of the type of intermediate results obtained when optimizing the pupil fraction metric PFWc (see Table 1 for a list of acronyms) is shown in Figure 6A. For each lens power over the range -1 to +1 D (in 0.125 D steps) a curve is generated relating RMS wavefront error to pupil radius. Each of these curves crosses the criterion level ($\lambda/4$ in our calculations) at some radius value. That radius is interpreted as the critical radius since it is the largest radius for which the eye's optical quality is reasonably good. The set of critical radius values can then be plotted as a function of defocus, as shown in Figure 6B. This through-focus function peaks at some value of

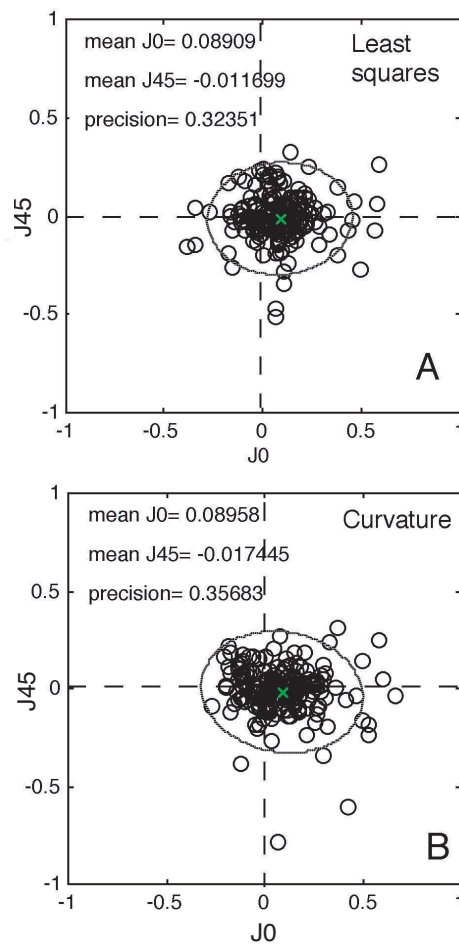


Figure 5. Scatter plots of (A) the least-squares fit of the wavefront over the entire pupil and (B) paraxial curvature matching methods of determining the two components of astigmatism. Circles show the results for individual eyes, green cross indicates the mean of the 2-dimensional distribution, and ellipses are 95% confidence intervals. Precision is the geometrical mean of the major and minor axes of the ellipse.

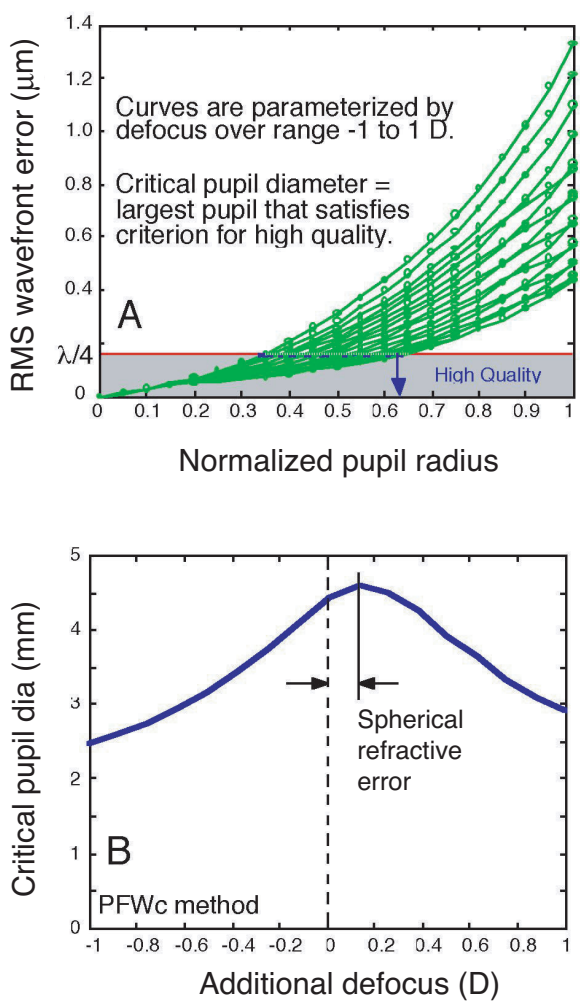


Figure 6. An example of intermediate results for the through-focus calculations needed to optimize the pupil fraction metric PFWc. (A) The RMS value is computed as a function of pupil radius for a series of defocus values added to the wavefront aberration function of this eye. The pupil size at the intersection points of each curve with the criterion level of RMS are plotted as a function of lens power in (B). The optimum correcting lens for this eye is the added spherical power that maximized the critical pupil diameter (and therefore maximized PFWc) which in this example is +0.125 D.

defocus, which is taken as the optimum lens for this eye using this metric. In this way the full dataset of Figure 6 is reduced to a single number.

Similar calculations were then repeated for other eyes in the population to yield 200 estimates of the refractive error using this particular metric. A frequency histogram of these 200 values similar to those in Figure 4 was produced for inspection by the experimenters. Such histograms were then summarized by a mean value, which we took to be a measure of accuracy, and a standard deviation, which (when doubled) was taken as a measure of precision.

The accuracy and precision of the 31 methods for objective refraction based on optimizing metrics of optical quality, plus the two methods based on wavefront fitting, are displayed in rank order in Figure 7. Mean accuracy varied from -0.50 D to +0.25 D. The 14 most accurate methods predicted M to within 1/8 D and 24 methods were accurate to within 1/4 D. The method of paraxial curvature matching was the most accurate method, closely followed by the through-focus method for maximizing the wavefront quality metrics PFWc and PFCT. Least-squares fitting was one of the least accurate methods (mean error = -0.39 D).

Precision of estimates of M ranged from 0.5 to 1.0 D. A value of 0.5 D means that the error in predicting M for 95 percent of the eyes in our study fell inside the confidence range given by the mean \pm 0.5 D. The most precise method was PFSc (± 0.49 D), which was statistically significant.

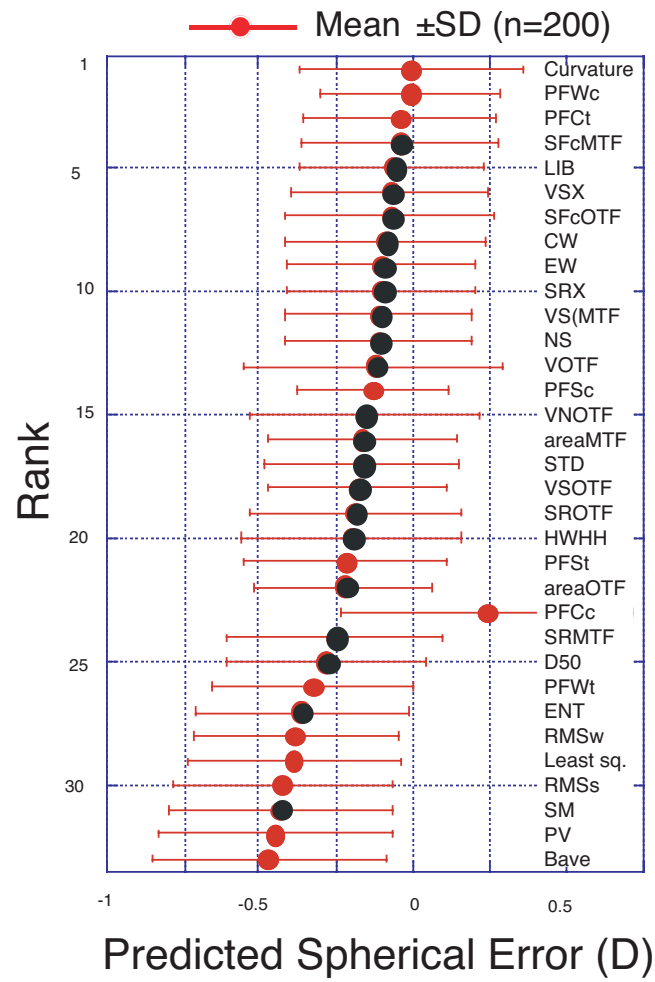


Figure 7. Rank ordering (based on accuracy) of 33 methods for predicting spherical refractive error. Red symbols indicate means for metrics based on wavefront quality. Black symbols indicate mean for metrics based on image quality. Error bars indicate ± 1 standard deviation of the population. Numerical data are given in Table 2.

cantly better than the others (*F*-test for equality of variance, 5% significance level). Precision of the next 14 methods in rank ranged from $\pm 0.58\text{D}$ to $\pm 0.65\text{D}$. These values were statistically indistinguishable from each other. This list of the 15 most precise methods included several examples from each of the three categories of wavefront quality, point-image quality, and grating-image quality. Rank ordering of all methods for predicting defocus is given in [Table 2](#).

A similar process was used to determine the accuracy for estimating astigmatism. We found that all methods except one (PFCc) had a mean error across the population of less than $1/8\text{ D}$. This accuracy is the best we could reasonably expect, given that the subjective refractions and the virtual refractions used to predict subjective refractions were both quantized at $1/8\text{ D}$ of cross-cylinder power. Precision of astigmatism predictions was typically better than precision for predicting defocus. The precision of all met-

rics for predicting astigmatism ranged from $\pm 0.32\text{D}$ to $\pm 1.0\text{D}$ and the 15 best methods were better than $\pm 0.5\text{D}$. Rank ordering of all methods for predicting astigmatism is given in [Table 3](#).

In comparing the precision for predicting defocus and astigmatism we found that 7 metrics were in the top-15 list for both types of prediction. Five of these were also accurate to within $1/8\text{ D}$ for predicting both defocus and astigmatism. Thus 5 metrics (PFSc, PFWc, VSMTF, NS, and PFCt) emerged as reasonably accurate and among the most precise. Three of these successful metrics were pupil plane metrics and two were image plane metrics. These results demonstrate that accurate predictions of subjective refractions are possible with pupil plane metrics. However, such metrics do not include the process of image formation that occurs in the eye, a process that must influence subjective image quality. For this reason, image-

Rank	Metric	Accuracy		Precision	
		Mean	Metric	2xSTD	Metric
1	PFCc	0.2406	PFSc	0.4927	
2	Curv	-0.006	AreaOTF	0.5803	
3	PFWc	-0.0063	VSOTF	0.5806	
4	PFCt	-0.0425	PFWc	0.5839	
5	SFcMTF	-0.0425	LIB	0.5951	
6	LIB	-0.0681	NS	0.5961	
7	VSX	-0.0731	VSMTF	0.5987	
8	SFcOTF	-0.0737	EW	0.6081	
9	CW	-0.0912	SRX	0.6081	
10	EW	-0.1006	AreaMTF	0.6112	
11	SRX	-0.1006	PFCt	0.6213	
12	VSMTF	-0.1131	STD	0.63	
13	NS	-0.1144	SFcMTF	0.6343	
14	VOTF	-0.125	VSX	0.6391	
15	PFSc	-0.1281	D50	0.6498	
16	VNOTF	-0.1575	CW	0.6558	
17	AreaMTF	-0.165	PFWt	0.6575	
18	STD	-0.1656	PFSt	0.6577	
19	VSOTF	-0.1794	RMSw	0.6702	
20	SROTF	-0.1875	SFcOTF	0.6786	
21	HWHH	-0.200	SRMTF	0.6888	
22	PFSt	-0.2162	SROTF	0.69	
23	AreaOTF	-0.2269	ENT	0.6987	
24	SRMTF	-0.2544	LSq	0.7062	
25	D50	-0.2825	HWHH	0.7115	
26	PFWt	-0.3231	RMSs	0.7159	
27	ENT	-0.3638	Curv	0.7202	
28	RMSw	-0.3831	SM	0.7315	
29	LSq	-0.3906	VNOTF	0.7486	
30	RMSs	-0.425	Bave	0.7653	
31	SM	-0.4319	PV	0.7725	
32	PV	-0.4494	VOTF	0.8403	
33	Bave	-0.4694	PFCc	0.9527	

Table 3. Rank ordering of methods for predicting spherical equivalent M based on accuracy and precision. Acronyms in red type are wavefront quality methods. Brief descriptions of acronyms are given in [Table 1](#). Detailed descriptions are in Appendix. Units are diopters.

Rank	Metric	Accuracy		Precision	
		Mean	Metric	2xSTD	Metric
1	HWHH	0.0155	LSq	0.3235	
2	LIB	0.0164	PFSc	0.3315	
3	PFCt	0.0192	Bave	0.3325	
4	AreaMTF	0.0258	RMSs	0.3408	
5	ENT	0.0273	RMSw	0.3429	
6	NS	0.0281	Curv	0.3568	
7	VSX	0.03	PFWc	0.3639	
8	PFSt	0.0305	PV	0.4278	
9	AreaOTF	0.0313	VSMTF	0.4387	
10	EW	0.0343	AreaMTF	0.4423	
11	SRX	0.0343	NS	0.4544	
12	SRMTF	0.038	PFCt	0.4715	
13	VSMTF	0.0407	STD	0.4752	
14	STD	0.0422	PFWt	0.4923	
15	CW	0.0576	SM	0.4967	
16	RMSs	0.0589	SRMTF	0.5069	
17	VSOTF	0.0594	EW	0.5181	
18	PFSc	0.0608	SRX	0.5181	
19	D50	0.0665	CW	0.5287	
20	SM	0.0668	LIB	0.535	
21	Bave	0.0685	AreaOTF	0.5444	
22	SROTF	0.0724	SFcMTF	0.5659	
23	PFWc	0.0745	VSX	0.5813	
24	VOTF	0.0787	VSOTF	0.6796	
25	LSq	0.0899	HWHH	0.6796	
26	RMSw	0.0909	SROTF	0.7485	
27	Curv	0.0913	PFSt	0.7555	
28	PV	0.098	SFcOTF	0.7821	
29	PFWt	0.1039	VNOTF	0.816	
30	VNOTF	0.1059	D50	0.8416	
31	SFcOTF	0.113	ENT	0.8751	
32	SFcMTF	0.1218	VOTF	0.9461	
33	PFCc	0.8045	PFCc	1.0005	

Table 2. Rank ordering of methods for predicting astigmatism parameters J_0 and J_{45} jointly. Acronyms in red type are wavefront quality methods. Brief descriptions of acronyms are given in [Table 1](#). Detailed descriptions are in Appendix. Units are diopters.

plane metrics of visual quality are more germane to vision models of the refraction process that seek to capture the subjective notion of a well-focused retinal image (Williams, Applegate, & Thibos, 2004).

Correlation between multiple objective refractions for the same eye

One implication of the results presented above is that different methods of objective refraction that yield similar refractions on average are likely to be statistically correlated. We tested this prediction by computing the correlation coefficient between all possible pairs of methods for predicting M . The resulting correlation matrix is visualized in Figure 8. For example, the left-most column of tiles in the matrix represents the Pearson correlation coefficient r between the first objective refraction method in the list (RMSw) and all other methods in the order specified in Table 1. Notice that the values of M predicted by optimizing RMSw are highly correlated with the values returned by methods 3 (RMSs), 8 (Bave), 19 (ENT), and 32 (least-squares fit). As predicted, all of these metrics are grouped at the bottom of the ranking in Figure 7. To the contrary, refractions using RMSw are poorly correlated with values returned by methods 4 (PFWc), 9 (PFCt), 21 (VSX), 24 (SFcOTF), and 33 (Curvature fit). All of these metrics are grouped at the top of the ranking in Figure 7, which further supports this connection between accuracy and correlation. A similar analysis of the correlation matrix for astigmatism parameters is not as informative because there was very little difference between the various methods for predicting J_0 and J_{45} .

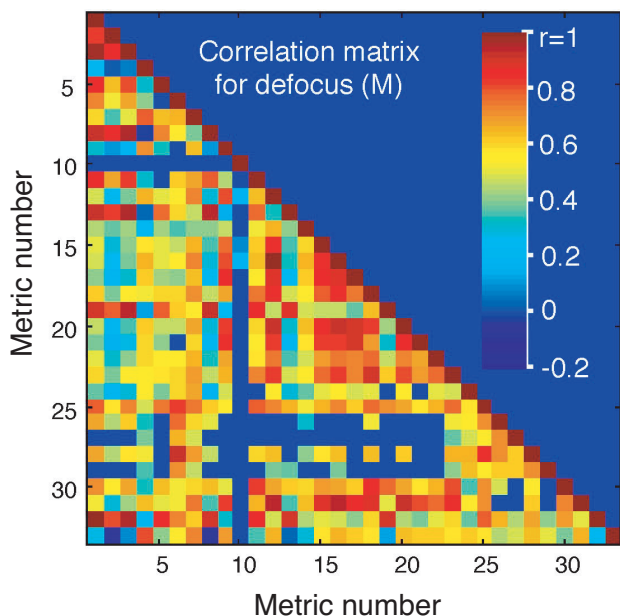


Figure 8. Correlation matrix for values of M determined by objective refraction. Metric number is given in Table 1.

Another interesting feature of Figure 8 is that some refraction methods (e.g. PFCc, VOTF, VNOTF) are very poorly correlated with all other methods. This result for metric PFCc is explained by the fact that PFCc was the only metric to produce hyperopic refractions in the vicinity of $M=+0.25D$. However, this argument does not apply to the other two examples that are poorly correlated with most other metrics even though these other metrics produced similar refractions on average (e.g. 20 (NS), 7 (PFS), and 23 (AreaMTF)). This result suggests that maximizing metrics VOTF and VNOTF optimizes a unique aspect of optical and visual quality that is missed by other metrics. In fact, these two metrics were specifically designed to capture infidelity of spatial phase in the retinal image.

Discussion

The least-squares method for fitting an aberrated wavefront with a spherical wavefront is the basis of Zernike expansion to determine the defocus coefficient. The failure of this method to accurately predict the results of subjective refraction implies that the Zernike coefficient for defocus is an inaccurate indicator of the spherical equivalent of refractive error determined by conventional subjective refractions. On average, this metric predicted that eyes in our study were myopic by $-0.39D$ when in fact they were well corrected.

To the contrary, matching paraxial curvature accurately predicted the results of subjective refraction. This method is closely related to the Seidel expansion of wavefronts because it isolates the purely parabolic (r^2) term. It also corresponds to a paraxial analysis since the r^2 coefficient is zero when the paraxial rays are well focused. Although this method was one of the least accurate methods for predicting astigmatism, it nevertheless was accurate to within $1/8D$. The curvature method was one of the most precise methods for predicting astigmatism but was significantly less precise than some other methods for predicting defocus. For this reason it was eliminated from the list of 5 most precise and accurate methods.

Figure 7 may be interpreted as a table of correction factors that could potentially make all of the predictions of defocus equally accurate. While this might seem a reasonable approach to improving accuracy, it may prove cumbersome in practice if future research should show that the correction factors vary with pupil diameter, age, or other conditions.

We do not know why the various metrics have different amounts of systematic bias, but at least two possibilities have already been mentioned. First, to undertake the data analysis we needed to make an assumption about which wavelength of light was well focused on the retina during subjective refraction with a polychromatic stimulus. We chose 570 nm as our reference wavelength based on theoretical and experimental evidence (Charman & Tucker, 1978; Thibos & Bradley, 1999) but the actual value is un-

known. Changing this reference wavelength by just 20 nm to 550 nm would cause a 0.1 D shift in defocus, which is a significant fraction of the differences in accuracy between the various metrics.

A second source of bias may be attributed to the difference between optimal and conventional refraction methods. The objective refraction procedures described in this paper are designed to determine the optimum refraction (Figure 1a) whereas the subjective refractions were conventional (Figure 1b). The difference between the two endpoints is half the depth-of-focus (DOF) of the eye. The DOF for subjects in the Indiana Aberration Study is unknown, but we would anticipate a value of perhaps ± 0.25 D (Atchison, Charman, & Woods, 1997) which is about half the total range of focus values spanned in Figure 7. Accordingly, we may account for the results in Figure 7 by supposing that the curvature matching technique happens to locate the far end of the DOF interval (which is located at optical infinity in a conventional refraction) whereas some middle-ranking metric (such as VSOTF) locates the middle of the DOF, located at the hyperfocal distance. This inference is consistent with the fact that most eyes in the Indiana Aberration Study had positive spherical aberration. Such eyes have less optical power for paraxial rays than for marginal rays. Consequently, the retina will appear to be conjugate to a point that is beyond the hyperfocal point if the analysis is confined to the paraxial rays.

The preceding arguments suggest that the superior accuracy of the curvature method for determining the spherical equivalent of a conventional refraction is due to a bias in this method that favors the far end of the eye's DOF. In short, *curvature matching (and several other metrics with similar accuracy) is a biased method that successfully predicts a biased endpoint*. By the same argument, the biased curvature method is not expected to predict astigmatism accurately because conventional refractions are unbiased for astigmatism. Although this line of reasoning explains why the paraxial curvature method will locate a point beyond the hyperfocal point, we lack a convincing argument for why the located point should lie specifically at infinity. Perhaps future experiments that include measurement of the DOF as well as the hyperfocal distance will clarify this issue and at the same time help identify objective methods for determining the hyperfocal distance.

Pursuing the above line of reasoning suggests that some metric near the bottom of the accuracy ranking, such as RMSw, locates the near end of the DOF. This accounting is consistent with the findings of Guirao and Williams (Guirao & Williams, 2003) and of Cheng *et al.* (Cheng, Bradley, & Thibos, 2004) that the optimum focus lies somewhere between the more distant paraxial focus and the nearer RMS focus. Taken together, the least-squares and curvature fitting methods would appear to locate the two ends of the DOF interval. While perhaps a mere coincidence, if this intriguing result could be substantiated theoretically then it might become a useful method to

compute the DOF from the wavefront aberration map for individual eyes.

A variety of other factors may also contribute to the range of inaccuracies documented in Figure 7. For example, all of the image quality metrics reported in this paper are based on monochromatic light. Generalizing these metrics to polychromatic light might improve the predictions of the subjective refraction. Inclusion of Stiles-Crawford apodization in the calculations might also improve the predictions. Also, it may be unrealistic to think that a single metric will adequately capture the multi-faceted notion of best-focus. A multi-variate combination of metrics which captures different aspects of optical image quality may yield better predictions (Williams *et al.*, 2004). Those metrics that included a neural component were configured with the same neural filter, when in fact different individuals are likely to have different neural filters. Furthermore, the characteristics of the neural filter are likely to depend on stimulus conditions. Koomen *et al.* (Koomen, Scolnik, & Tousey, 1951) and Charman *et al.* (Charman, Jennings, & Whitefoot, 1978) found that pupil size affects subjective refraction differently under photopic and scotopic illumination. They suggested that this might be due to different neural filters operating at photopic and scotopic light levels. A change in neural bandwidth of these filters would alter the relative weighting given to low and high spatial frequency components of the retinal image, thereby altering the optimum refraction. This idea suggests future ways to test the relative importance of the neural component of metrics of visual quality described here.

Variability in the gold standard of subjective refraction is another likely source of disagreement between objective and subjective refractions. The range of standard deviations for predicting M across all metrics was only 1/8 D (0.29–0.42 D), indicating that the precision of all metrics was much the same. This suggests that the precision of objective refraction might be dominated by a single, underlying source of variability. That source might in fact be variability in the subjective refraction. Bullimore *et al.* found that the 95% limit of agreement for repeatability of refraction is ± 0.75 D, which corresponds to a standard deviation of 0.375 D (Bullimore *et al.*, 1998). If the same level of variability were present in our subjective refractions, then uncertainty in determining the best subjective correction would have been the dominant source of error. It is possible, therefore, that all of our objective predictions are extremely precise but this precision is masked by imprecision of the gold standard of subjective refraction. If so, then an objective wavefront analysis that accurately determines the hyperfocal point and the DOF with reduced variability could become the new gold standard of refraction.

Comparison with companion studies

The metrics of image quality described in this paper have a potential utility beyond objective refraction. For example, Cheng *et al.* (Cheng *et al.*, 2004) and Marsack *et al.*

(Applegate, Marsack, & Thibos, 2004) both used the same implementation of these metrics described below (see Appendix) to predict the change in visual acuity produced when selected, higher-order aberrations are introduced into an eye. The experimental design of the Cheng study was somewhat simpler in that monochromatic aberrations were used to predict monochromatic visual performance, whereas Marsack used monochromatic aberrations to predict polychromatic performance. Nevertheless, both studies concluded that changes in visual acuity are accurately predicted by the pupil plane metric PFSt and by the image plane metric VSOTF. Furthermore, both studies concluded that three of the least accurate predictors were RMSw, HWHH, and VOTF. In addition, the Cheng study demonstrated that, as expected, those metrics which accurately predicted changes in visual acuity also predicted the lens power which maximized acuity in a through-focus experiment. This was an important result because it established a tight link between variations in monochromatic acuity and monochromatic refraction.

The superior performance of metric VSOTF is also consistent with the present study. This metric lies in the middle of the accuracy ranking for predicting M in a conventional refraction, which suggests that it would have accurately predicted M in an optimum refraction. (This point is illustrated graphically in Figure 5 of the Cheng *et al.* paper.) Furthermore, present results show that VSOTF is one of the most precise methods for estimating M, which suggests it is very good at monitoring the level of defocus in the retinal image for eyes with a wide variety of aberration structures. It follows that this metric should also be very good at tracking the loss of visual performance when images are blurred with controlled amounts of higher-order aberrations, as shown by the Cheng and Marsack studies. Lastly, the Cheng and Marsack studies rejected RMSw, HWHH, and VOTF as being among the least predictive metrics. All three of these metrics were among the least precise metrics for predicting M in the present study. It is reasonable to suppose that the high levels of variability associated with these metrics would have contributed to the poor performance recorded in those companion studies.

Appendix

This appendix summarizes a variety of metrics of visual quality of the eye. Several of these metrics are in common use, whereas others are novel. In the present study these metrics are used to estimate conventional refractions. Other studies have used these same metrics to estimate best focus for monochromatic letters (Cheng *et al.*, 2004) and to predict the change in visual acuity that results from the introduction of controlled amounts of selected, higher-order aberrations into polychromatic letters (Applegate *et al.*, 2004).

Metrics of wavefront quality

A perfect optical system has a flat wavefront aberration map and therefore metrics of wavefront quality are designed to capture the idea of flatness. An aberration map is flat if its value is constant, or if its slope or curvature is zero across the entire pupil. Since a wavefront, its slope, and its curvature each admits to a different optical interpretation, we sought meaningful scalar metrics based on all three: the wavefront aberration map, the slope map, and the curvature map. Programs for computing the metrics were written in Matlab (The Mathworks, Inc.) and tested against known examples.

Flatness metrics

Wavefront error describes optical path differences across the pupil that give rise to phase errors for light entering the eye through different parts of the pupil. These phase errors produce interference effects that degrade the quality of the retinal image. An example of a wave aberration map is shown in Figure A-1. Two common metrics of wavefront flatness follow.

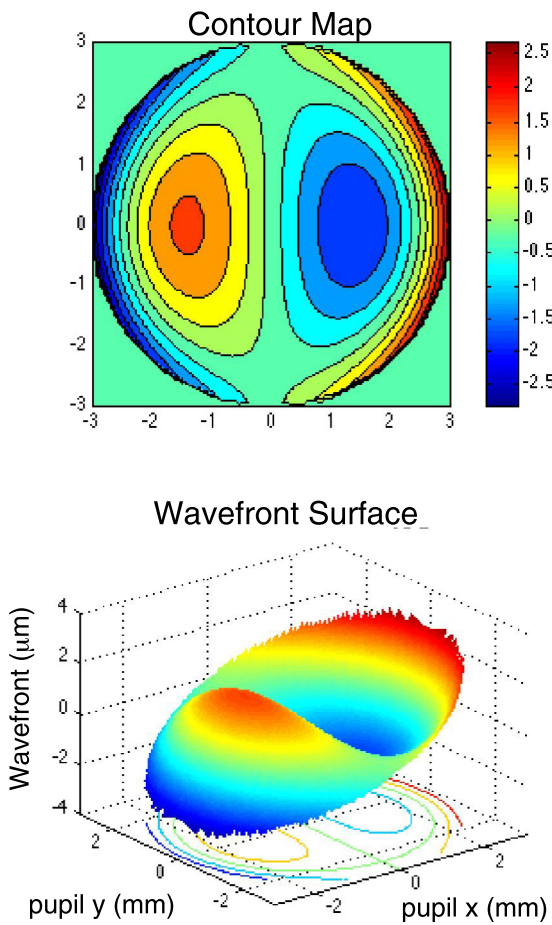


Figure A-1. A theoretical wavefront aberration map for 1 μm RMS of the third-order aberration coma over a 6 mm pupil.

RMS_w = root-mean-squared wavefront error computed over the whole pupil (microns)

$$RMS_w = \left[\frac{1}{A} \int_{pupil} (w(x,y) - \bar{w})^2 dx dy \right]^{0.5} \quad (A1)$$

where $w(x,y)$ is the wavefront aberration function defined over pupil coordinates x,y , A = pupil area, and the integration is performed over the domain of the entire pupil. Computationally, RMS_w is just the standard deviation of the values of wavefront error specified at various pupil locations.

PV = peak-to-valley difference (microns)

$$PV = \max(w(x,y)) - \min(w(x,y)) \quad (A2)$$

PV is the difference between the highest and lowest points in the aberration map.

Wavefront slope is a vector-valued function of pupil position that requires two maps for display, as illustrated in Figure A-2. One map shows the slope in the horizontal (x) direction and the other map shows the slope in the vertical (y) direction. (Alternatively, a polar-coordinate scheme would show the radial slope and tangential slope.) Wave-

front slopes may be interpreted as transverse ray aberrations that blur the image. These ray aberrations can be conveniently displayed as a vector field (lower right diagram). The base of each arrow in this plot marks the pupil location and the horizontal and vertical components of the arrow are proportional to the partial derivatives of the wavefront map. If the field of arrows is collapsed so that all the tails superimpose, the tips of the arrows represent a spot diagram (lower right diagram) that approximates the system point-spread function (PSF).

The root-mean-squared value of a slope map is a measure of the spreading of light rays that blur the image in one direction. The total RMS value computed for both slope maps taken together is thus a convenient metric of wavefront quality that may be interpreted in terms of the size of the spot diagram.

RMS_s = root-mean-squared wavefront slope computed over the whole pupil (arcmin)

$$RMS_s = \left[\frac{1}{A} \int_{pupil} (w_x(x,y) - \bar{w}_x)^2 + (w_y(x,y) - \bar{w}_y)^2 dx dy \right]^{0.5} \quad (A3)$$

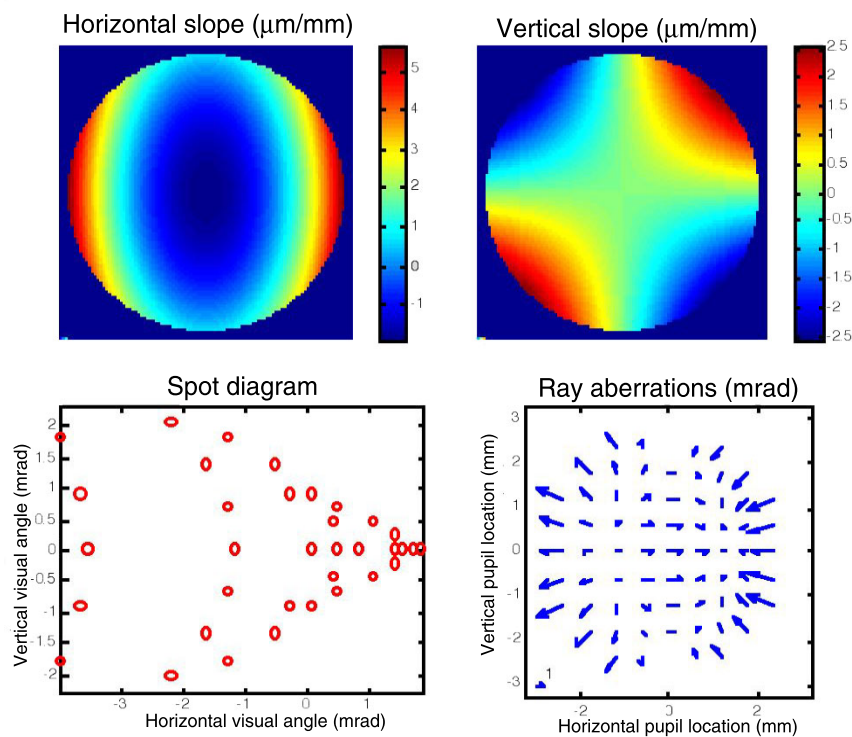


Figure A-2. Slope maps (upper row) are the partial derivatives of the wavefront map in Figure A-1. Information contained in these two maps is combined in the lower right diagram, which shows the magnitude and direction of ray aberrations at a regular grid of points in the pupil. The ray aberrations, in turn, can be used to generate the spot diagram in lower left. (Note, overlapping points in this example conceal the fact that there are as many points in the spot diagram as there are arrows in the ray aberration map.) Slopes are specified in units of milliradians (1 mrad = 3.44 arcmin).

where $w_x = dw/dx$ and $w_y = dw/dy$ are the partial spatial derivatives (i.e. slopes) of $w(x,y)$ and A = pupil area.

Wavefront curvature describes focusing errors that blur the image. To form a good image at some finite distance, wavefront curvature must be the same everywhere across the pupil. A perfectly flat wavefront will have zero curvature everywhere, which corresponds to the formation of a perfect image at infinity. Like wavefront slope, wavefront curvature is a vector-valued function of position that requires more than one map for display (Figure A-3). Curvature varies not only with pupil position but also with orientation at any given point on the wavefront.

Fortunately, Euler's classic formula of differential geometry assures us that the curvature in any meridian can be inferred from the principal curvatures (i.e. curvatures in the orthogonal meridians of maximum and minimum curvature) at the point in question (Carmo, 1976). The principal curvatures at every point can be derived from maps of mean curvature $M(x,y)$ and Gaussian curvature $G(x,y)$ as follows.

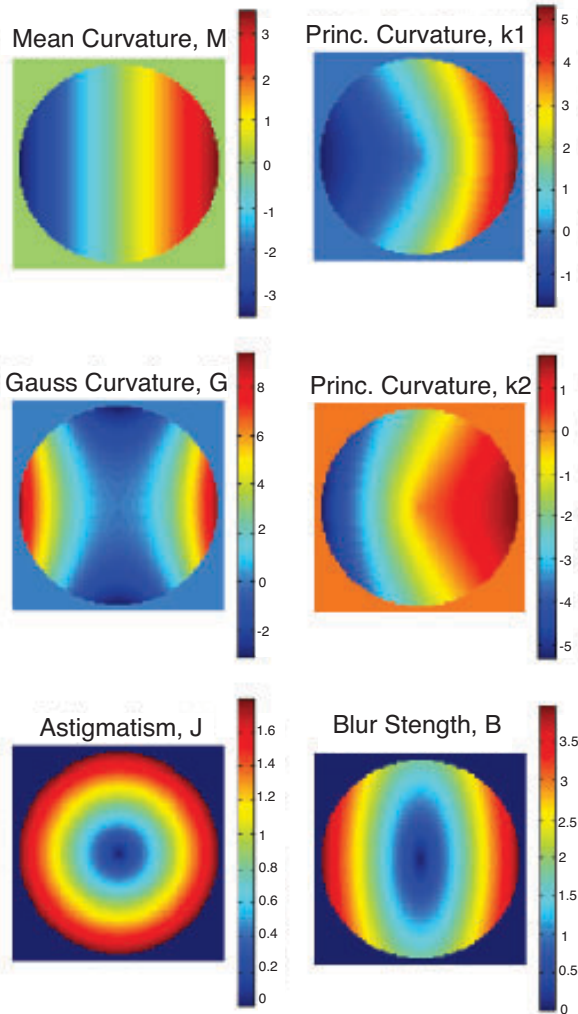


Figure A-3. Curvature maps derived from the wavefront in Figure 1. Calibration bars have units of diopters.

$$M(x,y) = \frac{k_1(x,y) + k_2(x,y)}{2} \quad (A4)$$

$$G(x,y) = k_1(x,y) \cdot k_2(x,y)$$

where the principal curvature maps $k_1(x,y)$, $k_2(x,y)$ are computed from M and G using

$$k_1, k_2 = M(x,y) \pm \sqrt{M^2(x,y) - G(x,y)} \quad (A5)$$

The Gaussian and mean curvature maps may be obtained from the spatial derivatives of the wavefront aberration map using textbook formulas (Carmo, 1976).

Given the principal curvature maps, we can reduce the dimensionality of wavefront curvature by computing blur strength at every pupil location. The idea of blur strength is to think of the wavefront locally as a small piece of a quadratic surface for which a power vector representation can be computed (Thibos et al., 1997). A power vector P (Bullimore et al., 1998) is a 3-dimensional vector whose coordinates correspond to the spherical equivalent (M), the normal component of astigmatism (J_0) and the oblique component of astigmatism (J_{45}). Experiments have shown that the length of the power vector, which is the definition of blur strength, is a good scalar measure of the visual impact of spherocylindrical blur (Raasch, 1995). Thus, a map of the length of the power-vector representation of a wavefront at each point in the pupil may be called a blur-strength map (Figure A-3).

To compute the blur-strength map we first use the principal curvature maps to compute the astigmatism map

$$J(x,y) = \frac{k_1(x,y) - k_2(x,y)}{2} \quad (A6)$$

and then combine the astigmatism map with the mean curvature map using the Pythagorean formula to produce a blur strength map

$$B(x,y) = \sqrt{M^2(x,y) + J^2(x,y)} \quad (A7)$$

The spatial average of this blur strength map is a scalar value that represents the average amount of focusing error in the system that is responsible for image degradation,

$$B_{ave} = \text{average blur strength (diopters)}$$

$$B_{ave} = \frac{1}{\text{pupil area}} \int_{\text{pupil}} B(x,y) dx dy \quad (A8)$$

Pupil fraction metrics

In addition to the 4 metrics described above, another 6 metrics of wavefront quality can be defined based on the concept of *pupil fraction*. Pupil fraction is defined as the

fraction of the pupil area for which the optical quality of the eye is reasonably good (but not necessarily diffraction-limited). A large pupil fraction is desirable because it means that most of the light entering the eye will contribute to a good-quality retinal image.

$$\text{Pupil Fraction} = \frac{\text{Area of good pupil}}{\text{Total area of pupil}} \quad (\text{A9})$$

Two general methods for determining the area of the good pupil are illustrated in Figure A-4. The first method, called the critical pupil or central pupil method, examines the wavefront inside a sub-aperture that is concentric with the eye's pupil (Corbin, Klein, & van de Pol, 1999; Howland & Howland, 1977). We imagine starting with a small sub-aperture where image quality is guaranteed to be good (i.e. diffraction-limited) and then expanding the aperture until some criterion of wavefront quality is reached. This endpoint is the *critical diameter*, which can be used to compute the pupil fraction (critical pupil method) as follows

$$PF_c = \left[\frac{\text{critical diameter}}{\text{pupil diameter}} \right]^2 \quad (\text{A10})$$

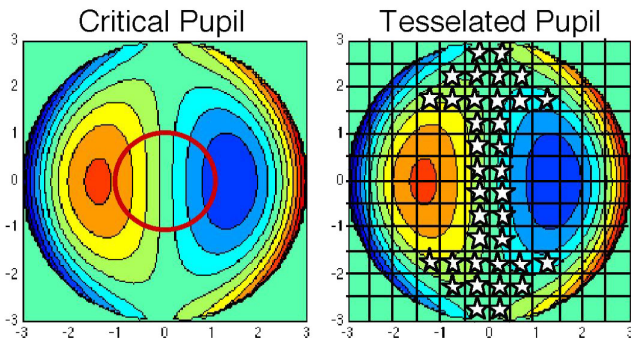


Figure A-4. Pupil fraction method for specifying wavefront quality. Red circle in the left diagram indicates the largest concentric sub-aperture for which the wavefront has reasonably good quality. White stars in the right diagram indicate subapertures for which the wavefront has reasonably good quality.

To implement Equation 10 requires some criterion for what is meant by good wavefront quality. For example, the criterion could be based on the wavefront aberration map,

$$PFW_c = PF_c \text{ when critical pupil is defined as the concentric area for which } RMS_w < \text{criterion (e.g. } \lambda/4)$$

Alternatively, the criterion for good wavefront quality could be based on wavefront slope,

$$PFS_c = PF_c \text{ when critical pupil is defined as the concentric area for which } RMS_s < \text{criterion (e.g. 1 arcmin)}$$

Or the criterion could be based on wavefront curvature as represented by the blur strength map,

$$PFC_c = PF_c \text{ when critical pupil is defined as the concentric area for which } B_{ave} < \text{criterion (e.g. 0.25D)}$$

The second general method for determining the area of the good pupil is called the tessellation or whole pupil method. We imagine tessellating the entire pupil with small sub-apertures (about 1% of pupil diameter) and then labeling each sub-aperture as good or bad according to some criterion (Figure A-4, right-hand diagram). The total area of all those sub-apertures labeled good defines the area of the good pupil from which we compute pupil fraction as

$$PF_t = \frac{\text{Area of good subapertures}}{\text{Total area of pupil}} \quad (\text{A11})$$

As with the concentric metrics, implementation of Equation 11 requires criteria for deciding if the wavefront over a sub-aperture is good. For example, the criterion could be based on the wavefront aberration function,

$$PFW_t = PF_t \text{ when a good sub-aperture satisfies the criterion } PV < \text{criterion (e.g. } \lambda/4)$$

Alternatively, the criterion could be based on wavefront slope,

$$PFS_t = PF_t \text{ when a good sub-aperture satisfies the criterion horizontal slope and vertical slope are both } < \text{criterion (e.g. 1 arcmin)}$$

Or the criterion could be based on wavefront curvature as summarized by blur strength,

$$PFC_t = PF_t \text{ when a good sub-aperture satisfies the criterion } B < \text{criterion (e.g. 0.25D)}$$

Metrics of image quality for point objects

A perfect optical system images a point object into a compact, high-contrast retinal image as illustrated in Figure A-5. The image of a point object is called a point-spread function (PSF). The PSF is calculated as the squared magnitude of the inverse Fourier transform of the pupil function $P(x,y)$, defined as

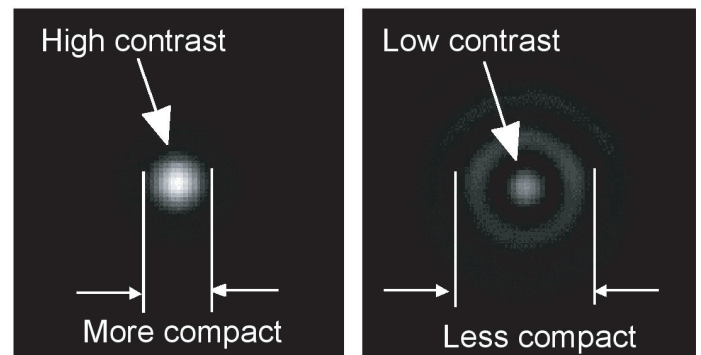


Figure A-5. Measures of image quality for point objects are based on contrast and compactness of the image.

$$P(x, y) = A(x, y) \exp(ikW(x, y)) \quad (\text{A12})$$

where k is the wave number ($2\pi/\text{wavelength}$) and $A(x, y)$ is an optional apodization function of pupil coordinates x, y . When computing the physical retinal image at the entrance apertures of the cone photoreceptors, the apodization function is usually omitted. However, when computing the visual effectiveness of the retinal image, the waveguide nature of cones must be taken into account. These waveguide properties cause the cones to be more sensitive to light entering the middle of the pupil than to light entering at the margin of the pupil (Burns, Wu, Delori, & Elsner, 1995; Roorda & Williams, 2002; Stiles & Crawford, 1933). It is common practice to model this phenomenon as an apodizing filter with transmission $A(x, y)$ in the pupil plane (Atchison, Joblin, & Smith, 1998; Bradley & Thibos, 1995; Zhang, Ye, Bradley, & Thibos, 1999).

Scalar metrics of image quality that measure the quality of the PSF in aberrated eyes are designed to capture the dual attributes of compactness and contrast. The first 5 metrics listed below measure spatial compactness and in every case small values of the metric indicate a compact PSF of good quality. The last 6 metrics measure contrast and in every case large values of the metric indicate a high-contrast PSF of good quality. Most of the metrics are completely optical in character, but a few also include knowledge of the neural component of the visual system. Several of these metrics are 2-dimensional extensions of textbook metrics defined for 1-dimensional impulse response functions (Bracewell, 1978). Many of the metrics are normalized by diffraction-limited values and therefore are unitless.

Compactness metrics

D50 = diameter of a circular area centered on PSF peak which captures 50% of the light energy (arcmin)

The value of D50 is equal to the radius r , where r is defined implicitly by:

$$\int_0^{2\pi} \int_0^r PSF_N(r, \theta) r dr d\theta = 0.5 \quad (\text{A13})$$

where PSF_N is the normalized (i.e. total intensity = 1) point-spread function with its peak value located at $r = 0$. This metric ignores the light outside the central 50% region, and thus is insensitive to the shape of the PSF tails.

EW = equivalent width of centered PSF (arcmin)

The equivalent width of the PSF is the diameter of the circular base of that right cylinder which has the same volume as the PSF and the same height. The value of EW is given by:

$$EW = \left[\frac{4 \int_{\text{pupil}} PSF(x, y) dx dy}{\pi PSF(x_0, y_0)} \right]^{0.5} \quad (\text{A14})$$

where x_0, y_0 are the coordinates of the peak of the PSF. In this and following equations, x, y are spatial coordinates of the retinal image, typically specified as visual angles subtended at the eye's nodal point. Note that although EW describes spatial compactness, it is computed from PSF contrast. As the height falls the width must increase to maintain a constant volume under the PSF.

SM = square root of second moment of light distribution (arcmin)

This metric is analogous to the moment of inertia of a distribution of mass. It is computed as

$$SM = \left[\frac{\int_{\text{pupil}} (x^2 + y^2) PSF(x, y) dx dy}{\int_{\text{pupil}} PSF(x, y) dx dy} \right]^{0.5} \quad (\text{A15})$$

Unlike D50 above, this compactness metric is sensitive to the shape of the PSF tails. Large values of SM indicate a rapid roll-off of the optical transfer function at low spatial frequencies (Bracewell, 1978).

HWHH = half width at half height (arcmin)

This metric is the average width of every cross-section of the PSF. It is computed as

$$HWHH = \left[\frac{1}{\pi} \int_{\text{pupil}} C(x, y) dx dy \right]^{0.5} \quad (\text{A16})$$

where $C(x, y) = 1$ if $PSF(x, y) > \max(PSF)/2$, otherwise $C(x, y) = 0$. A 1-dimensional version of this metric has been used on line spread functions of the eye (Charman & Jennings, 1976; Westheimer & Campbell, 1962).

CW = correlation width of light distribution (arcmin)

This metric is the HWHH of the autocorrelation of the PSF. It is computed as

$$CW = \left[\frac{1}{\pi} \int_{-\infty}^{\infty} \int_{-\infty}^{\infty} Q(x, y) dx dy \right]^{0.5} \quad (\text{A17})$$

where $Q(x, y) = 1$ if $PSF \otimes PSF > \max(PSF \otimes PSF)/2$, otherwise $Q(x, y) = 0$. In this expression, $PSF \otimes PSF$ is the autocorrelation of the PSF.

Contrast metrics

SRX = Strehl ratio computed in spatial domain

This widely-used metric is typically defined with respect to the peak of the PSF, rather than the coordinate origin. It is computed as

$$SRX = \frac{\max(PSF)}{\max(PSF_{DL})} \quad (A18)$$

where PSF_{DL} is the diffraction-limited PSF for the same pupil diameter.

LIB = light-in-the-bucket

The value of this metric is the percentage of total energy falling in an area defined by the core of a diffraction-limited PSF,

$$LIB = \int_{DL\ core} PSF_N(x, y) dx dy \quad (A19)$$

where PSF_N is the normalized (i.e. total intensity = 1) point-spread function. The domain of integration is the central core of a diffraction-limited PSF for the same pupil diameter. An alternative domain of interest is the entrance aperture of cone photoreceptors. Similar metrics have been used in the study of depth-of-focus (Marcos, Moreno, & Navarro, 1999).

STD = standard deviation of intensity values in the PSF, normalized to diffraction-limited value

This metric measures the variability of intensities at various points in the PSF,

$$STD = \frac{\left[\int_{psf} \left(PSF(x, y) - \overline{PSF} \right)^2 dx dy \right]^{0.5}}{\left[\int_{psf} \left(PSF_{DL}(x, y) - \overline{PSF}_{DL} \right)^2 dx dy \right]^{0.5}} \quad (A20)$$

where PSF_{DL} is the diffraction-limited point-spread function. The domain of integration is a circular area centered on the PSF peak and large enough in diameter to capture most of the light in the PSF.

ENT = entropy of the PSF

This metric is inspired by an information-theory approach to optics (Guirao & Williams, 2003).

$$ENT = - \int_{psf} PSF(x, y) \ln(PSF(x, y)) dx dy \quad (A21)$$

NS = neural sharpness

This metric was introduced by Williams as a way to capture the effectiveness of a PSF for stimulating the neural portion of the visual system (Williams, 2003). This is achieved by weighting the PSF with a spatial sensitivity function that represents the neural visual system. The product is then integrated over the domain of the PSF. Here we normalize the result by the corresponding value for a diffraction-limited PSF to achieve a metric that is analogous to the Strehl ratio computed for a neurally-weighted PSF,

$$NS = \frac{\int_{psf} PSF(x, y) g(x, y) dx dy}{\int_{psf} PSF_{DL}(x, y) g(x, y) dx dy} \quad (A22)$$

where $g(x, y)$ is a bivariate-Gaussian, neural weighting-function. A profile of this weighting function (Figure A-6) shows that it effectively ignores light outside of the central 4 arc minutes of the PSF.

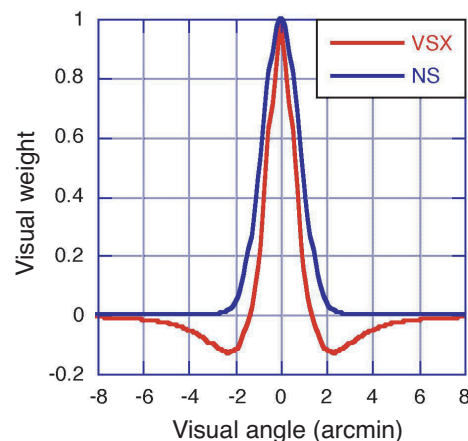


Figure A-6. Neural weighting functions used by NS and VSX.

VSX = visual Strehl ratio computed in the spatial domain.

Like the neural sharpness metric, the visual Strehl ratio is an inner product of the PSF with a neural weighting function normalized to the diffraction-limited case. The difference between NS and VSX is in the choice of weighting functions (Figure A-6).

$$VSX = \frac{\int_{psf} PSF(x, y) N(x, y) dx dy}{\int_{psf} PSF_{DL}(x, y) N(x, y) dx dy} \quad (A23)$$

where $N(x,y)$ is a bivariate neural weighting function equal to the inverse Fourier transform of the neural contrast sensitivity function for interference fringes (Campbell & Green, 1965). With this metric, light outside of the central 3 arc minutes of the PSF doubly detracts from image quality because it falls outside the central core and within an inhibitory surround. This is especially so for light just outside of the central 3 arc minutes in that slightly aberrated rays falling 2 arc minutes away from the PSF center are more detrimental to image quality than highly aberrated rays falling farther from the center.

Metrics of image quality for grating objects

Unlike point objects, which can produce an infinite variety of PSF images depending on the nature of the eye's aberrations, small patches of grating objects always produce sinusoidal images no matter how aberrated the eye. Consequently, there are only two ways that aberrations can affect the image of a grating patch: they can reduce the contrast or translate the image sideways to produce a phase-shift, as illustrated in Figure A-7. In general, the amount of contrast attenuation and the amount of phase shift both depend on the gratings spatial frequency. This variation of image contrast with spatial frequency for an object with 100% contrast is called a modulation transfer function (MTF). The variation of image phase shift with spatial frequency is

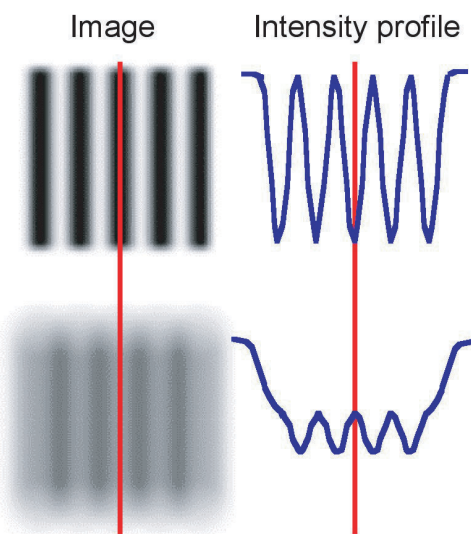


Figure A-7. Measures of image quality for grating objects are based on contrast and phase shifts in the image. Upper row depicts a high-quality image of a grating object. Lower row depicts a low quality image with reduced contrast and a 180 deg phase shift. Left column shows the grating images and right column show horizontal traces of intensity through the corresponding images. Red lines are reference marks that highlight the phase shifts that can occur in blurred images.

called a phase transfer function (PTF). Together, the MTF and PTF comprise the eye's optical transfer function (OTF). The OTF is computed as the Fourier transform of the PSF.

Optical theory tells us that any object can be conceived as the sum of gratings of various spatial frequencies, contrasts, phases and orientations. In this context we think of the optical system of the eye as a filter that lowers the contrast and changes the relative position of each grating in the object spectrum as it forms a degraded retinal image. A high-quality OTF is therefore indicated by high MTF values and low PTF values. Scalar metrics of image quality in the frequency domain are based on these two attributes of the OTF.

SFcMTF = spatial frequency cutoff of radially-averaged modulation-transfer function (rMTF)

Cutoff SF is defined here as the intersection of the radially averaged MTF (rMTF) and the neural contrast threshold function (Thibos, 1987). The rMTF is computed by integrating the full 2-dimensional MTF over orientation. This metric does not capture spatial phase errors in the image because rMTF is not affected by the PTF portion of the OTF.

SFcMTF = highest spatial freq. for which
rMTF > neural threshold (A24)

where

$$rMTF(f) = \frac{1}{2\pi} \int_0^{2\pi} \text{abs}(OTF(f, \phi)) d\phi \quad (\text{A25})$$

and $OTF(f, \phi)$ is the optical transfer function for spatial frequency coordinates f (frequency) and ϕ (orientation). A graphical depiction of SFcMTF is shown in Figure A-8.

SFcOTF = spatial frequency cutoff of radially-averaged optical-transfer function (rOTF).

The radially-averaged OTF is determined by integrating the full 2-dimensional OTF over orientation. Since the PTF component of the OTF is taken into account when computing rOTF, this metric is intended to capture spatial phase errors in the image.

SFcOTF = lowest spatial freq. for which
rOTF < neural threshold (A26)

where

$$rOTF(f) = \frac{1}{2\pi} \int_0^{2\pi} OTF(f, \phi) d\phi .$$

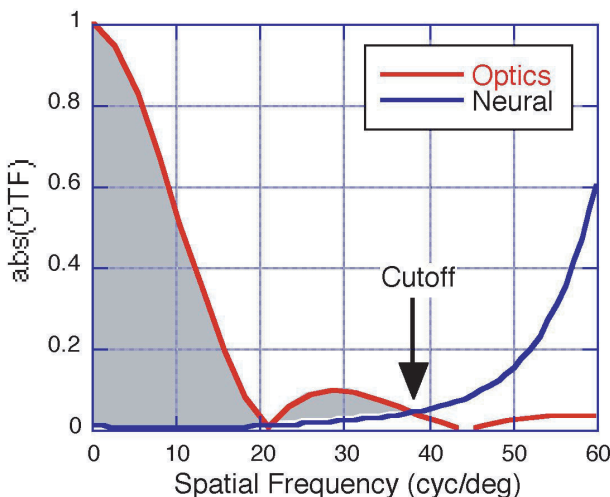


Figure A-8. Radial MTF for a defocused optical system, showing intersection with neural threshold function that defines cutoff spatial frequency metric SFcMTF. Shaded area below the MTF and above the neural threshold is the area of visibility specified in the definition of metric AreaMTF.

and $OTF(f,\phi)$ is the optical transfer function for spatial frequency coordinates f (frequency) and ϕ (orientation). Since the OTF is a complex-valued function, integration is performed separately for the real and imaginary components. Conjugate symmetry of the OTF ensures that the imaginary component vanishes, leaving a real-valued result. A graphical depiction of SFcOTF is shown in Figure A-9.

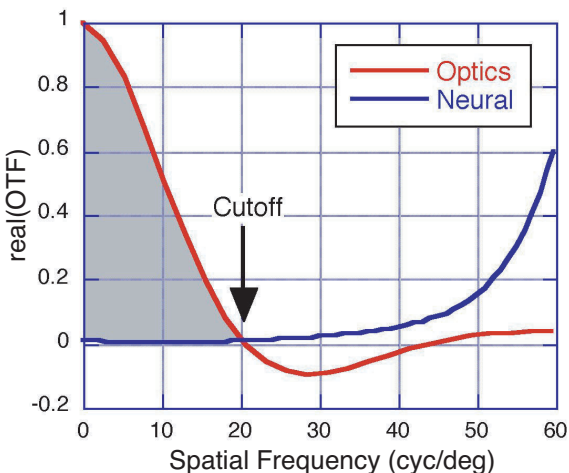


Figure A-9. Radial OTF for a defocused optical system, showing intersection with neural threshold function to define cutoff spatial frequency metric SFcOTF. Shaded area below the OTF and above the neural threshold is the area of visibility specified in the definition of metric AreaOTF.

The primary distinction between metrics SFcMTF and SFcOTF is that SFcMTF ignores phase errors, with phase-altered and even phase-reversed modulations treated the same as correct-phase modulations. For example, with an amplitude-oscillating and phase-reversing defocused OTF, the SFcMTF identifies the highest frequency for which modulation exceeds threshold, irrespective of lower frequency modulation minima and phase reversals (Figure A-8). By contrast, SFcOTF identifies the highest SF within the correct-phase, low-frequency portion of the OTF (Figure A-9). This allows spurious resolution to be discounted when predicting visual performance on tasks of spatial resolution and pattern discrimination.

AreaMTF = area of visibility for rMTF (normalized to diffraction-limited case).

The area of visibility in this context is the region lying below the radially averaged MTF and above the neural contrast threshold function (Charman & Olin, 1965; Mouroulis, 1999). The normalized metric is computed as

$$AreaMTF = \frac{\int_0^{cutoff} rMTF(f) df - \int_0^{cutoff} T_N(f) df}{\int_0^{cutoff} rMTF_{DL}(f) df - \int_0^{cutoff} T_N(f) df} \quad (A27)$$

where T_N is the neural contrast threshold function, which equals the inverse of the neural contrast sensitivity function (Campbell & Green, 1965). When computing area under rMTF, phase-reversed segments of the curve count as positive area (Figure A-8). This is consistent with our definition of SFcMTF as the highest frequency for which rMTF exceeds neural threshold. This allows spurious resolution to be counted as beneficial when predicting visual performance for the task of contrast detection. Metrics based on the volume under the MTF have been used in studies of chromatic aberration (Marcos, Burns, Moreno-Barriusop, & Navarro, 1999) and visual instrumentation (Mouroulis, 1999).

AreaOTF = area of visibility for rOTF (normalized to diffraction-limited case).

The area of visibility in this context is the region that lies below the radially averaged OTF and above the neural contrast threshold function. The normalized metric is computed as

$$AreaOTF = \frac{\int_0^{cutoff} rOTF(f) df - \int_0^{cutoff} T_N(f) df}{\int_0^{cutoff} rOTF_{DL}(f) df - \int_0^{cutoff} T_N(f) df} \quad (A28)$$

where T_N is the neural contrast threshold function defined above. Since the domain of integration extends only to the cutoff spatial frequency, phase-reversed segments of the curve do not contribute to area under rOTF. This is consistent with our definition of SFcOTF as the lowest frequency for which rOTF is below neural threshold. This metric would be appropriate for tasks in which phase reversed modulations (spurious resolution) actively interfere with performance.

SRMTF = Strehl ratio computed in frequency domain (MTF method)

The Strehl ratio is often computed in the frequency domain on the strength of the central ordinate theorem of Fourier analysis (Bracewell, 1978). This theorem states that the central value of a function is equal to the area (or volume, in the 2-dimensional case) under its Fourier transform. Since the OTF is the Fourier transform of the PSF, we may conclude that the volume under the OTF is equal to the value of the PSF at the coordinate origin. In many cases the PTF portion of the OTF is unknown, which has led to the popular substitution of the MTF for the OTF in this calculation. Although popular, this method lacks rigorous justification because $MTF=|OTF|$. This non-linear transformation destroys the Fourier-transform relationship between the spatial and frequency domains that is the basis of the central ordinate theorem, which in turn is the justification for computing Strehl ratio in the frequency domain.

$$SRMTF = \frac{\int_{-\infty}^{\infty} \int_{-\infty}^{\infty} MTF(f_x, f_y) df_x df_y}{\int_{-\infty}^{\infty} \int_{-\infty}^{\infty} MTF_{DL}(f_x, f_y) df_x df_y} \quad (A29)$$

Strehl ratio computed by the MTF method is equivalent to the Strehl ratio for a hypothetical PSF that is well-centered with even symmetry computed as the inverse Fourier transform of MTF (which implicitly assumes. PTF=0). Thus, in general, SRMTF is only an approximation of the actual Strehl ratio computed in the spatial domain (SRX).

SROTF = Strehl ratio computed in frequency domain (OTF method)

The Strehl ratio computed by the OTF method will accurately compute the ratio of heights of the PSF and a diffraction-limited PSF at the coordinate origin. However, the peak of the PSF does not necessarily occur at the coordinate origin established by the pupil function. Consequently, the value of SROTF is not expected to equal SRX exactly, except in those special cases where the peak of the PSF occurs at the coordinate origin.

$$SROTF = \frac{\int_{-\infty}^{\infty} \int_{-\infty}^{\infty} OTF(f_x, f_y) df_x df_y}{\int_{-\infty}^{\infty} \int_{-\infty}^{\infty} OTF_{DL}(f_x, f_y) df_x df_y} \quad (A30)$$

VSMTF = visual Strehl ratio computed in frequency domain (MTF method)

This metric is similar to the MTF method of computing the Strehl ratio, except that the MTF is weighted by the neural contrast sensitivity function CSF_N ,

$$VSMTF = \frac{\int_{-\infty}^{\infty} \int_{-\infty}^{\infty} CSF_N(f_x, f_y) \cdot MTF(f_x, f_y) df_x df_y}{\int_{-\infty}^{\infty} \int_{-\infty}^{\infty} CSF_N(f_x, f_y) \cdot MTF_{DL}(f_x, f_y) df_x df_y} \quad (A31)$$

In so doing, modulation in spatial frequencies above the visual cut-off of about 60 c/deg is ignored, and modulation near the peak of the CSF (e.g. 6 c/deg) is weighted maximally. It is important to note that this metric gives weight to visible, high spatial-frequencies employed in typical visual acuity testing (e.g. 40 c/deg in 20/15 letters). Visual Strehl ratio computed by the MTF method is equivalent to the visual Strehl ratio for a hypothetical PSF that is well-centered with even symmetry computed as the inverse Fourier transform of MTF (which implicitly assumes. PTF=0). Thus, in general, VSMTF is only an approximation of the visual Strehl ratio computed in the spatial domain (VSX).

VSOTF = visual Strehl ratio computed in frequency domain (OTF method)

This metric is similar to the OTF method of computing the Strehl ratio, except that the OTF is weighted by the neural contrast sensitivity function CSF_N ,

$$VSOTF = \frac{\int_{-\infty}^{\infty} \int_{-\infty}^{\infty} CSF_N(f_x, f_y) \cdot OTF(f_x, f_y) df_x df_y}{\int_{-\infty}^{\infty} \int_{-\infty}^{\infty} CSF_N(f_x, f_y) \cdot OTF_{DL}(f_x, f_y) df_x df_y} \quad (A32)$$

This metric differs from VSX by emphasizing image quality at the coordinate origin, rather than at the peak of the PSF.

VOTF = volume under OTF normalized by the volume under MTF

This metric is intended to quantify phase shifts in the image. It does so by comparing the volume under the OTF to the volume under the MTF.

$$VOTF = \frac{\int_{-\infty}^{\infty} \int_{-\infty}^{\infty} OTF(f_x, f_y) df_x df_y}{\int_{-\infty}^{\infty} \int_{-\infty}^{\infty} MTF(f_x, f_y) df_x df_y} \quad (\text{A33})$$

Since the MTF \geq the real part of the OTF, this ratio is always ≤ 1 . Creation of this metric was inspired by a measure of orientation bias of the receptive fields of retinal ganglion cells introduced by Thibos & Levick (Exp. Brain Research, 58:1-10, 1985).

VNOTF = *volume under neurally-weighted OTF, normalized by the volume under neurally-weighted MTF*

This metric is intended to quantify the visually-significant phase shifts in the image. It does so by weighting the MTF and OTF by the neural contrast sensitivity function before comparing the volume under the OTF to the volume under the MTF.

$$VNOTF = \frac{\int_{-\infty}^{\infty} \int_{-\infty}^{\infty} CSF_N(f_x, f_y) \cdot OTF(f_x, f_y) df_x df_y}{\int_{-\infty}^{\infty} \int_{-\infty}^{\infty} CSF_N(f_x, f_y) \cdot MTF(f_x, f_y) df_x df_y} \quad (\text{A34})$$

Polychromatic metrics

The wavefront aberration function is a monochromatic concept. If a source emits polychromatic light, then wavefront aberration maps for each wavelength are treated separately because lights of different wavelengths are mutually incoherent and do not interfere. For this reason, the definition of metrics of wavefront quality do not generalize easily to handle polychromatic light. Nevertheless, it is possible to compute the value of a given metric for each wavelength in a polychromatic source and then form a weighted average of the results,

$$\text{Metric}_{poly} = \int V(\lambda) \text{Metric}(\lambda) d\lambda \quad (\text{A35})$$

where the weighting function $V(\lambda)$ is the luminous efficiency function that describes how visual sensitivity to monochromatic light varies with wavelength λ .

To the contrary, polychromatic metrics of image quality for point objects are easily defined by substituting polychromatic images for monochromatic images. For example, the polychromatic luminance point-spread function PSF_{poly} is a weighted sum of the monochromatic spread functions $PSF(x,y,\lambda)$,

$$PSF_{poly} = \int V(\lambda) PSF(x, y, \lambda) d\lambda \quad (\text{A36})$$

Given this definition, PSF_{poly} may be substituted for PSF in any of the equations given above to produce new, polychromatic metrics of image quality. In addition to these luminance metrics of image quality, other metrics can be devised to capture the changes in color appearance of the image caused by ocular aberrations. For example, the chromaticity coordinates of a point source may be compared to the chromaticity coordinates of each point in the retinal PSF and metrics devised to summarize the differences between image chromaticity and object chromaticity. Such metrics may prove useful in the study of color vision.

Given the polychromatic point-spread function defined above in [Equation A-36](#), a polychromatic optical transfer function OTF_{poly} may be computed as the Fourier transform of PSF_{poly} . Substituting this new function for OTF (and its magnitude for MTF) in any of the equations given above will produce new metrics of polychromatic image quality defined in the frequency domain. Results obtained by these polychromatic metrics will be described in a future report.

Correlation between metrics

Since all of the metrics of wavefront and image quality defined above are intended to measure the optical quality of an eye, they are expected to be statistically correlated. To estimate the degree of correlation for normal healthy eyes, we computed each of these monochromatic, non-apodized metrics for all 200 well refracted eyes of the Indiana Aberration Study (Thibos, Hong, Bradley, & Cheng, [2002](#)). The correlation matrix for all 31 metrics of optical quality is shown in [Figure A-10](#). Only a few correlations were found to be statistically insignificant ($\alpha=0.05$) and these were coded as zero in the figure.

Given the strong correlations between metrics evident in [Figure A-10](#), the question arose whether it would be possible to discover a smaller set of uncorrelated variables that could adequately account for the individual variability in our study population. To answer this question we used principal component (PC) analysis (Jackson, [1991](#)). This analysis indicated that a single PC with the largest characteristic root can account for 65% of the variance between eyes. This first PC is an orthogonal regression line that is a “line of best fit” since it provides the best account of between-eye variation of the individual metrics. For our normal, well-corrected eyes the first PC gave approximately equal weighting to all 31 metrics except VOTF (which had about 1/4 the weight of the other metrics). This implies that inter-subject variability of metric values (relative to the mean) is about the same for each metric yet each metric emphasizes a different aspect of optical quality. The sign of the weighting was positive for metrics that increase as optical quality increases and negative for metrics that decrease as optical quality increases. Thus, PC#1 may be interpreted as an overall metric of optical quality.

One practical use of principal component analysis in this context is to identify unusual eyes for which the vari-

ous metrics of optical quality do not agree. This outlier analysis is done formally by computing Hotelling's T-squared statistic for each eye and flagging those values that are abnormally large (Jackson, 1991).

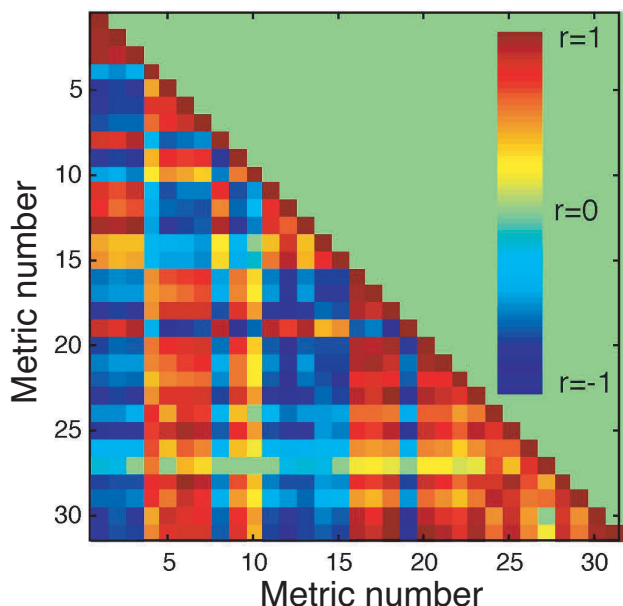


Figure A-10. Correlation matrix. Each square indicates the correlation coefficient for the corresponding pair of metrics. Color bar indicates scale of correlation coefficient. Ordering of metrics is given in Table 1.

Acknowledgments

This research was supported by National Institutes of Health Grant EY-05109 (LNT) and EY 08520 (RAA). We thank the authors of the Indiana Aberration Study for access to their aberration database. We thank Jacob Rubenstein for help with differential geometry issues, Xu Cheng for critical comments and help with figure production, and Austin Roorda for suggesting the through-focus virtual-refraction paradigm.

Commercial relationships: Thibos and Applegate have a proprietary interest in the development of optical metrics predictive of visual performance.

Corresponding author: Larry Thibos.

Email: thibos@indiana.edu.

Address: Indiana University, School of Optometry, Bloomington, IN, USA.

References

- Applegate, R. A., Ballantine, C., Gross, H., Sarver, E. J., & Sarver, C. A. (2003). Visual acuity as a function of Zernike mode and level of root mean square error. *Optometry and Vision Science*, 80(2), 97-105. [PubMed]
- Applegate, R. A., Marsack, J. D., Ramos, R., & Sarver, E. J. (2003). Interaction between aberrations to improve or reduce visual performance. *Journal of Cataract and Refractive Surgery*, 29(8), 1487-1495. [PubMed]
- Atchison, D. A., Charman, W. N., & Woods, R. L. (1997). Subjective depth-of-focus of the eye. *Optometry and Vision Science*, 74(7), 511-520. [PubMed]
- Atchison, D. A., Joblin, A., & Smith, G. (1998). Influence of Stiles-Crawford effect apodization on spatial visual performance. *Journal of the Optical Society of America A*, 15(9), 2545-2551. [PubMed]
- Bland, J. M., & Altman, D. G. (1986). Statistical methods for assessing agreement between two methods of clinical measurement. *Lancet*, 1(8476), 307-310. [PubMed]
- Borisch, I. M. (1970). *Clinical Refraction* (Vol. 1). Chicago: The Professional Press, Inc.
- Bracewell, R. N. (1978). *The Fourier Transform and Its Applications* (2nd ed.). New York: McGraw-Hill.
- Bradley, A., & Thibos, L. N. (1995). Modeling off-axis vision – I: the optical effects of decentering visual targets or the eye's entrance pupil. In E. Peli (Ed.), *Vision Models for Target Detection and Recognition* (Vol. 2, pp. 313-337). Singapore: World Scientific Press. [Article]
- Bullimore, M. A., Fusaro, R. E., & Adams, C. W. (1998). The repeatability of automated and clinician refraction. *Optometry and Vision Science*, 75(8), 617-622. [PubMed]
- Burns, S. A., Wu, S., Delori, F., & Elsner, A. E. (1995). Direct measurement of human-cone-photoreceptor alignment. *Journal of the Optical Society of America A*, 12(10), 2329-2338. [PubMed]
- Campbell, F. W. (1957). The depth of field of the human eye. *Optica Acta*, 4, 157-164.
- Campbell, F. W., & Green, D. G. (1965). Optical and retinal factors affecting visual resolution. *Journal of Physiology*, 181, 576-593. [PubMed]
- Carmo, M. P. (1976). *Differential Geometry of Curves and Surfaces*. Englewood Cliffs, NJ: Prentice-Hall.
- Charman, N., & Jennings, J. A. M. (1976). The optical quality of the monochromatic retinal image as a function of focus. *British Journal of Physiological Optics*, 31, 119-134.
- Charman, N., Jennings, J. A. M., & Whitefoot, H. (1978). The refraction of the eye in relation to spherical aberration and pupil size. *British Journal of Physiological Optics*, 32, 78-93.
- Charman, N., & Olin, A. (1965). Image quality criteria for aerial camera systems. *Photographic Science and Engineering*, 9, 385-397.
- Charman, W. N., & Tucker, J. (1978). Accommodation and color. *Journal of the Optical Society of America*, 68, 459-471.

- Cheng, X., Bradley, A., & Thibos, L. N. (2004). Predicting subjective judgment of best focus with objective image quality metrics. *Journal of Vision*, 4(4), 310-321, <http://journalofvision.org/4/4/7/>, doi:10.1167/4.4.7. [PubMed] [Article]
- Cheng, X., Thibos, L. N., & Bradley, A. (2003). Estimating visual quality from wavefront aberration measurements. *Journal of Refractive Surgery*, 19, S579-S584. [Article]
- Corbin, J. A., Klein, S., & van de Pol, C. (1999). Measuring effects of refractive surgery on corneas using Taylor series polynomials. In P. O. Rol & K. M. Joos & F. Manns & B. E. Stuck & M. Belkin (Eds.), *Proceedings of SPIE* (Vol. 3591, pp. 46-52).
- Enoch, J. M., & Lakshminarayanan, V. (1991). Retinal Fiber Optics. In W. N. Charman (Ed.), *Vision Optics and Instrumentation* (1 ed., Vol. 1, pp. 280-308). London, U.K.: MacMillan Press.
- Fienup, J. R., & Miller, J. J. (2003). Aberration correction by maximizing generalized sharpness metrics. *Journal of the Optical Society of America A*, 20, 609-620. [PubMed]
- Guirao, A., & Williams, D. R. (2003). A method to predict refractive errors from wave aberration data. *Optometry and Vision Science*, 80(1), 36-42. [PubMed]
- Howland, H. C., & Howland, B. (1977). A subjective method for the measurement of monochromatic aberrations of the eye. *Journal of the Optical Society of America*, 67(11), 1508-1518. [PubMed]
- Hultgren, B. O. (1990). Subjective quality factor revisited. *Proceedings of the SPIE*, 1249, 12-22.
- Jackson, J. E. (1991). *A User's Guide to Principal Components*. New York: John Wiley & Sons.
- King, W. B. (1968). Dependence of the Strehl ratio on the magnitude of the variance of the wave aberration. *Journal of the Optical Society of America*, 58, 655-661.
- Koomen, M., Scolnik, R., & Tousey, R. (1951). A study of night myopia. *Journal of the Optical Society of America*, 41, 80-90.
- Mahajan, V. N. (1991). *Aberration Theory Made Simple* (Vol. TT6). Bellingham, WA: SPIE Optical Engineering Press.
- Marcos, S., Burns, S. A., Moreno-Barriusop, E., & Navarro, R. (1999). A new approach to the study of ocular chromatic aberrations. *Vision Research*, 39(26), 4309-4323. [PubMed]
- Marcos, S., Moreno, E., & Navarro, R. (1999). The depth-of-field of the human eye from objective and subjective measurements. *Vision Research*, 39(12), 2039-2049. [PubMed]
- Marsack, J. D., Thibos, L. N., & Applegate, R. A. (2004). Metrics of optical quality derived from wave aberrations predict visual performance. *Journal of Vision*, 4(4), 322-328, <http://journalofvision.org/4/4/8/>, doi:10.1167/4.4.8. [PubMed] [Article]
- Metcalf, H. (1965). Stiles-Crawford apodization. *Journal of the Optical Society of America*, 55, 72-74.
- Mouroulis, P. (1999). Aberration and image quality representation for visual optical systems. In P. Mouroulis (Ed.), *Visual Instrumentation: Optical Design and Engineering Principle* (pp. 27-68). New York: McGraw-Hill.
- Raasch, T. W. (1995). Spherocylindrical refractive errors and visual acuity. *Optometry and Vision Science*, 72, 272-275. [PubMed]
- Roorda, A., & Williams, D. R. (2002). Optical fiber properties of individual human cones. *Journal of Vision*, 2(5), 404-412, <http://journalofvision.org/2/5/4/>, doi:10.1167/2.5.4. [PubMed] [Article]
- Stiles, W. S., & Crawford, B. H. (1933). The luminous efficiency of rays entering the pupil at different points. *Proceedings of the Royal Society of London (B)*, 112, 428-450.
- Thibos, L. N. (1987). Calculation of the influence of lateral chromatic aberration on image quality across the visual field. *Journal of the Optical Society of America A*, 4, 1673-1680. [PubMed]
- Thibos, L. N., Applegate, R. A., Schwiegerling, J. T., & Webb, R. (2000). Standards for reporting the optical aberrations of eyes. In V. Lakshminarayanan (Ed.), *Trends in Optics and Photonics* (Vol. 35, pp. 232-244). Washington, D.C.: Optical Society of America, reprinted in *Journal of Refractive Surgery* 18, S652-S660 (2002). [Slideshow]
- Thibos, L. N., & Bradley, A. (1995). Modeling off-axis vision - II: the effect of spatial filtering and sampling by retinal neurons. In E. Peli (Ed.), *Vision Models for Target Detection and Recognition* (Vol. 2, pp. 338-379). Singapore: World Scientific Press. [Article]
- Thibos, L. N., & Bradley, A. (1999). Modeling the refractive and neuro-sensor systems of the eye. In P. Mouroulis (Ed.), *Visual Instrumentation: Optical Design and Engineering Principle* (pp. 101-159). New York: McGraw-Hill. [Article]
- Thibos, L. N., Bradley, A., & Applegate, R. A. (2002). *Where is the far-point in an aberrated eye?* [Abstract] *Journal of Vision*, 2(10), 41a, <http://journalofvision.org/2/10/41/>, doi:10.1167/2.10.41. [Slideshow]
- Thibos, L. N., Hong, X., & Bradley, A. (2001). *Predicting visual performance from scalar metrics of optical quality*. Paper presented at the OSA Annual Meeting, Long Beach, CA. [Slideshow]

- Thibos, L. N., Hong, X., Bradley, A., & Cheng, X. (2002). Statistical variation of aberration structure and image quality in a normal population of healthy eyes. *Journal of the Optical Society of America, A*, 19, 2329-2348. [PubMed] [Article]
- Thibos, L. N., Wheeler, W., & Horner, D. G. (1997). Power vectors: an application of Fourier analysis to the description and statistical analysis of refractive error. *Optometry and Vision Science*, 74, 367-375. [PubMed] [Article]
- Thibos, L. N., Ye, M., Zhang, X., & Bradley, A. (1992). The chromatic eye: a new reduced-eye model of ocular chromatic aberration in humans. *Applied Optics*, 31, 3594-3600.
- Westheimer, G., & Campbell, F. W. (1962). Light distribution in the image formed by the living human eye. *Journal of the Optical Society of America*, 52, 1040-1045.
- Williams, D. R. (2003). Subjective image quality metrics from the wave aberration. Paper presented at the 4th International Congress of Wavefront Sensing and Aberration-Free Refractive Correction, San Francisco, CA.
- Williams, D. R., Applegate, R. A., & Thibos, L. N. (2004). Metrics to predict the subjective impact of the eye's wave aberration. In R. R. Krueger, Applegate, R. A., MacRae, S.M. (Ed.), *Wavefront Customized Visual Correction: The Quest for Super Vision II* (pp. 78-84). Thorofare, NJ: Slack.
- Zhang, X., Ye, M., Bradley, A., & Thibos, L. N. (1999). Apodization by the Stiles-Crawford effect moderates the visual impact of retinal image defocus. *Journal of the Optical Society of America, A*, 16, 812-820. [PubMed] [Article]